

Certifiable Estimation with Factor Graphs

Zhexin Xu, Nikolas R. Sanderson, Hanna Jiamei Zhang, and David M. Rosen, *Senior Member, IEEE*

Abstract—Factor graphs provide a convenient modular modeling language that enables practitioners to easily design and deploy a wide range of high-performance robotic state estimation systems by composing simple, reusable building blocks; however, inference in these models is typically performed using *local* optimization methods that can converge to suboptimal solutions, a serious reliability concern in safety-critical applications. Conversely, *certifiable estimators* based upon convex relaxation are capable of recovering *verifiably globally optimal* solutions of challenging estimation problems in many practical settings; however, the computational cost of solving the large-scale relaxations they employ necessitates the use of specialized, structure-exploiting solvers that require substantial effort and specialized expertise to implement, which has to date significantly hampered their practical deployment.

In this paper, we show that these two paradigms, which have thus far been treated as essentially independent in the literature, can be naturally synthesized into a unified framework for *certifiable factor graph optimization*. The key insight enabling this synthesis is that factor graph structure is *preserved* under Shor’s relaxation and Burer-Monteiro factorization: applying these transformations to a QCQP with an associated factor graph representation yields a lifted problem that admits a factor graph model with *identical* connectivity, in which the variables and factors are simple one-to-one algebraic transformations (*lifts*) of those appearing in the original QCQP. We show that this structural preservation enables the Riemannian Staircase methodology for certifiable estimation to be implemented and deployed using the same mature, highly-performant factor graph libraries and workflows already ubiquitously employed throughout robotics and computer vision, making certifiable estimation as straightforward to design and deploy as conventional factor graph inference.

Index Terms—Factor graphs, certifiable estimation, semidefinite optimization, Burer-Monteiro factorization, Riemannian Staircase, SLAM

I. INTRODUCTION

STATE estimation is the problem of inferring the values of some unknown parameters of interest from (typically noisy) sensor data. This is a foundational capability in mobile robotics, supporting such basic functions as perception, planning, navigation, and control [1], [2]. Canonical examples of state estimation problems in robotics include *simultaneous localization and mapping* (SLAM) [3], [4] and *structure from motion* (SfM) [5], among many others.

Factor graphs provide a powerful framework for modeling state estimation problems in robotics and computer vision [6]. These models are based upon the insight that the estimation

tasks arising in robotic state estimation applications are typically composed of a limited set of recurring parameters (e.g. 3D points and robot poses) and measurement types (such as visual, inertial, or LiDAR observations). Given mathematical descriptions of these elementary parameters and sensing modalities, factor graphs provide a convenient, modular modeling language that enables even complex, high-dimensional state estimation problems to be easily and naturally expressed by composing these simple constituent parts.

Factor graphs have consequently become the dominant paradigm for modeling and solving state estimation problems in robotics and computer vision, with several commonly-used state-of-the-art software libraries based upon this abstraction [7]–[9]. Given a factor graph model of a state estimation task, these libraries typically formalize the inference problem as *maximum likelihood estimation* (MLE) or *maximum a posteriori estimation* (MAP) [6], and then apply smooth local optimization methods to compute a point estimate. This approach is attractive from a computational standpoint, as it admits the use of fast first- or second-order smooth numerical optimization algorithms [10] to compute these point estimates efficiently; indeed, it enables processing estimation problems involving tens to hundreds of thousands of states on a single processor in real-time [8], [9], [11], [12]. Furthermore, it is straightforward to algorithmically synthesize and run a fast local optimization algorithm directly from the factor graph specification of an estimation task; from an operational standpoint, this enables practitioners to focus their attention exclusively on *modeling* the task to be solved (i.e. *what* to do), rather than on the minutiae of designing efficient inference algorithms for the resulting problem formulation (i.e. *how* to do it). However, this computational and operational expedience comes at the cost of *reliability*: because this approach is based upon *local* optimization, the recovered estimates lack guarantees of *correctness* (i.e. *global* optimality). Although accurate estimates can often be obtained with careful initialization [13], the absence of formal performance guarantees remains a serious limitation of this approach, especially in safety-critical applications.

Alternatively, *certifiably correct* estimation algorithms have recently emerged as a powerful class of techniques for robustly solving challenging state estimation tasks [4]. These techniques are based upon *convex relaxation* rather than local search: they proceed by constructing a convex (typically *semidefinite*) *approximation* of an MLE or MAP problem instance, and then (*globally*) solving this convex surrogate to produce a point estimate. Remarkably, a growing body of work has shown that this approach is capable of efficiently recovering *exact, verifiably globally optimal* solutions to challenging estimation tasks in many practical settings. However, despite their tremendous potential, at present certifiably correct

The authors are with the Robust Autonomy Lab, Institute for Experiential Robotics, Northeastern University, 360 Huntington Ave, Boston, MA 02115, USA. {xu.zhexin, sanderson.n, zhang.hanna, d.rosen}@northeastern.edu. We acknowledge the support of the Natural Sciences and Engineering Research Council of Canada (NSERC). Nous remercions le Conseil de recherches en sciences naturelles et en génie du Canada (CRSNG) de son soutien.

estimators can be prohibitively difficult to design and deploy in practice. In particular, these methods frequently require the solution of large-scale semidefinite relaxations that are far beyond the capabilities of off-the-shelf general-purpose (interior-point) optimization algorithms [14], necessitating the use of more scalable *custom built, structure exploiting* techniques. At present, the design and implementation of these specialized semidefinite optimization methods requires substantial subject matter expertise in convex analysis and numerical optimization, along with significant problem-specific manual analysis, design, and implementation effort. These practical implementation challenges present a serious barrier to the more widespread exploration and development of certifiable methods within the research community, as well as their deployment in real-world systems (particularly for practitioners without highly-specialized expertise in applied mathematics).

In this paper, we describe a simple approach to designing, implementing, and deploying a wide variety of certifiable estimators using the same factor graph modeling and *local* optimization paradigm (and associated software libraries) already ubiquitously employed throughout robotics and computer vision. The main idea behind our approach is to exploit the connection between a factor graph model of an estimation problem formulated as a quadratically-constrained quadratic program (QCQP) and the Burer-Monteiro factorization [15] of its associated semidefinite relaxation. Specifically, we show that one can apply simple algebraic transformations (*lifts*) to the individual variables and factors appearing in the original factor graph model of the QCQP to produce a corresponding factor graph model for the Burer-Monteiro-factored semidefinite relaxation. This result implies that the Burer-Monteiro-factored relaxation can be instantiated and locally optimized using existing factor graph libraries augmented with *certifiable* (lifted) variants of standard variable and factor types. When applied in combination with the Riemannian Staircase methodology [16], our approach thus enables practitioners to easily synthesize and deploy *certifiable* estimators using current state-of-the-art factor graph-based software libraries and workflows. Experimental evaluation on a variety of geometric estimation tasks demonstrates that certifiable estimators implemented using our factor graph-based approach preserve the computational speed of current state-of-the-art *local* factor graph optimization methods while also enabling the recovery of *certifiably globally optimal solutions*. Moreover, our framework dramatically reduces the engineering effort necessary to design and implement these certifiable estimators, from the order of *months* to *hours*.

In summary, the key contributions of this work are:

- 1) We elucidate the connection between a factor graph model of a quadratically-constrained quadratic program and a factor graph model of the Burer-Monteiro factorization of its associated Shor relaxation. Specifically, we show that the latter can be constructed by applying simple algebraic transformations (*lifts*) to the individual variables and factors appearing in the former. This result implies that it is possible to instantiate and *locally* optimize these Burer-Monteiro factorizations using existing factor graph-based software libraries augmented with lifted variants of

standard variable and factor types.

- 2) We show how to solve the Shor relaxation via the Riemannian Staircase methodology, using our certifiable factor graph framework to instantiate and *locally* optimize the (inner) Burer-Monteiro-factored semidefinite programs in each iteration. This framework thus enables practitioners to easily design and deploy certifiable estimators using existing factor graph-based software libraries and workflows.
- 3) We provide concrete descriptions of the lifts of several types of variables (points, rotations, and unit vectors) and factors (relative rotations, rigid motions, pose-to-point measurements, and point-to-point ranges) commonly encountered in robotic mapping and navigation tasks.
- 4) We release an open-source C++ implementation of our approach integrated into GTSAM.¹

The rest of this paper is organized as follows. We begin by surveying related work in Section III. Next, we briefly review the factor graph paradigm as commonly applied to solve state estimation problems in robotics and computer vision (in Section IV), and the construction of certifiable optimization methods for quadratically-constrained quadratic programs via the Riemannian Staircase methodology (in Section V), as these form the foundation of our approach. Section VI presents our main technical contributions: we show how one can easily design and deploy certifiable estimators using factor graphs to model and *locally* optimize the Burer-Monteiro-factored semidefinite programs appearing in each level of the Riemannian Staircase. We apply these results to obtain concrete descriptions of the lifted variants of several common variable and factor types (in Section VII), and then show how one can use these lifted types to implement certifiable estimators for several common estimation tasks in robotic navigation (Section VIII). Finally, Section IX concludes with a summary of this paper’s contributions and a discussion of future research directions.

II. NOTATION

In this section we fix some notation that will be useful throughout the remainder of the paper. Given an integer $n > 0$, we write $[n] \triangleq \{1, \dots, n\}$ to denote the set of integers from 1 to n (inclusive). Similarly, given an n -tuple $x = (x_1, \dots, x_n)$ and a subset $S = \{i_1, \dots, i_k\} \subseteq [n]$ of size k with $i_1 < \dots < i_k$, we define x_S to be the k -tuple whose elements are indexed by the elements of S :

$$x_S \triangleq (x_{i_1}, \dots, x_{i_k}). \quad (1)$$

We write \mathbb{R} to denote the set of real numbers. Similarly, given an integer $n > 0$ we denote by \mathbb{S}^n and \mathbb{S}_+^n the sets of symmetric and symmetric positive-semidefinite matrices of size $n \times n$ (respectively). We write $O(d)$, $SO(d)$, and $SE(d)$ for the *orthogonal*, *special orthogonal*, and *special Euclidean* groups acting on d -dimensional Euclidean space

¹We will provide a link to our implementation following peer review.

(respectively). We will identify $O(d)$ and $SO(d)$ with their realizations as the following matrix Lie groups:

$$O(d) \triangleq \{R \in \mathbb{R}^{d \times d} \mid R^T R = I_d\}, \quad (2)$$

$$SO(d) \triangleq \{R \in \mathbb{R}^{d \times d} \mid R^T R = I_d, \det(R) = +1\}, \quad (3)$$

and $SE(d)$ with its realization as the semidirect product $SE(d) \cong \mathbb{R}^d \rtimes SO(d)$, with group operations:

$$(t_1, R_1) \cdot (t_2, R_2) = (t_1 + R_1 t_2, R_1 R_2), \quad (4a)$$

$$(t, R)^{-1} = (-R^{-1}t, R^{-1}). \quad (4b)$$

Similarly, given integers k and n with $1 \leq k \leq n$, we let

$$St(k, n) \triangleq \{X \in \mathbb{R}^{n \times k} \mid X^T X = I_k\} \quad (5)$$

denote the set of ordered orthonormal k -frames in n -dimensional Euclidean space; this set forms a smooth compact matrix manifold called the *Stiefel manifold* [17]. Finally, we write S^n to denote the n -dimensional unit sphere centered on the origin in $(n+1)$ -dimensional Euclidean space:

$$S^n \triangleq \{x \in \mathbb{R}^{n+1} \mid \|x\|_2 = 1\}. \quad (6)$$

Note that comparing (2) and (6) with (5) reveals that the orthogonal group and the unit sphere are themselves specific instances of Stiefel manifolds:

$$S^n = St(1, n+1), \quad O(n) = St(n, n). \quad (7)$$

III. RELATED WORK

Many robotic perception and state estimation problems are naturally formalized as optimization problems via maximum likelihood estimation (MLE) or M-estimation [6]. This formulation offers a simple, flexible, and general framework with strong statistical performance guarantees under mild conditions. However, the resulting optimization problems are often nonconvex and high-dimensional, and thus computationally hard (i.e. NP-hard) to solve in general.

Because solving MLE problems is computationally intractable in general, current state-of-the-art robotic perception and state estimation methods typically resort to *local* (rather than *global*) optimization. Most M-estimation problems arising in robotics and computer vision are smooth optimization problems defined over a product of smooth manifolds [4] and can thus be *locally* optimized very efficiently using smooth first- or second-order sparsity-exploiting optimization algorithms [18]. Factor graphs provide a simple, modular modeling language for describing even large-scale instances of these problems by composing simple constituent parts. Moreover, it is straightforward to algorithmically synthesize and deploy fast local optimization algorithms directly from a factor graph model of an M-estimation problem [6]; indeed, current state-of-the-art techniques built on these principles can easily process problems involving ten- to hundred-thousand-dimensional states on single threads in real-time [8], [9], [11], [12], [19]. However, because this approach is based upon *local* (rather than *global*) search, it is susceptible to convergence to significantly suboptimal local minima. The practical consequence is that current state-of-the-art techniques based upon *local* search often return egregiously wrong estimates *without*

warning. This lack of reliability is a serious concern in safety-critical applications such as autonomous vehicles, drones, and aerospace systems.

Alternatively, recent work has led to the development of a new class of *certifiably correct* estimation algorithms that are capable of recovering *certifiably globally optimal* solutions to challenging estimation problems in many practical settings [20]–[22]. The main idea behind these methods is to replace *local* optimization with *convex relaxation*: these methods proceed by constructing a *convex approximation* to the target estimation problem, and then (*globally*) solving this convex surrogate to recover a point estimate for the original estimation problem. Remarkably, recent work has shown (both theoretically and empirically) that the solutions returned by these methods are often *exact, globally optimal* solutions to the original estimation task; moreover, whenever exactness occurs, it is possible to verify this fact *a posteriori* by constructing a *computational certificate of correctness* for the recovered estimate. Certifiably correct methods thus provide a mathematically rigorous and (in principle) computationally efficient approach for reliable robotic perception.

However, despite their tremendous promise, at present certifiable estimation methods remain difficult to design and deploy, primarily due to the high computational cost of solving the large-scale convex (typically *semidefinite*) relaxations that they employ. Standard off-the-shelf interior-point SDP solvers [23], [24] do not scale well beyond problems with a few thousand dimensions; however, many foundational robotic perception and state estimation problems, such as pose graph optimization [25] and bundle adjustment [26], involve tens to hundreds of thousands of dimensions, making direct application of these solvers impractical.

To address this computational challenge, prior work has explored several strategies for improving the scalability of SDP optimization methods. One approach involves approximating the SDP cone itself via simpler convex relaxations such as linear programs (LPs), second-order cone programs (SOCPs), or sum-of-squares hierarchies like DSOS and SDSOS [27]. While these approximate methods can be very effective at reducing computational complexity, they do not guarantee the recovery of an exact solution to the original SDP, potentially sacrificing the very exactness and certifiability properties that motivated our use of semidefinite relaxations for certifiable estimation. Another common approach is *chordal decomposition*, which decomposes a large SDP into smaller interconnected SDPs, reducing the size of the largest matrix variable and thus the primary computational bottleneck. However, chordal decomposition is commonly implemented via consensus-ADMM, a first-order optimization method with sublinear convergence rates that can exhibit prohibitively slow convergence on badly conditioned problems [28]. Many problems of interest in robotics, such as pose graph optimization and bundle adjustment, are known to be very badly conditioned, making chordal decomposition impractically slow for these applications.

The most effective approach to date for implementing large-scale certifiable estimation methods is *Burer-Monteiro (BM) factorization* [15], [16]. Rather than optimizing over the full semidefinite matrix, BM factorization exploits the existence

of low-rank solutions by searching directly for a low-rank factors. This reduces the search from a high-dimensional positive semidefinite matrix to low-dimensional factors, yielding significant memory savings (from $\mathcal{O}(n^3)$ to $\mathcal{O}(np^2)$, where $p \ll n$ is the chosen rank of the factorization) and reformulating the optimization as a standard low-dimensional nonlinear program (NLP). Critically, this allows the use of fast second-order NLP methods of the same type already employed in factor graph optimization. These methods are known to be efficient in practice and handle bad numerical conditioning much better than first-order methods [18]. Notably, essentially all examples of large-scale certifiable estimators for geometric perception tasks that have appeared in the literature to date are built upon this framework [20], [29]–[33].

However, at present BM-factorization-based certifiable estimators are difficult to deploy. The NLPs arising in this approach are nonconvex, requiring more complex meta-algorithms such as the Riemannian Staircase [20] to guarantee convergence to an optimal low-rank factor for the original SDP. Moreover, to achieve fast computation, most current state-of-the-art implementations rely on intrinsic, on-manifold Riemannian optimization algorithms [34], which must be custom-tailored to the geometry of each specific problem instance’s feasible set. Consequently, at present, implementing a fast, scalable, Riemannian optimization-based BM-factored certifiable estimator is incredibly laborious: practitioners must manually analyze the SDP relaxation, derive the Shor relaxation, construct the BM factorization, design a custom Riemannian optimization algorithm, and wrap this in a Riemannian Staircase meta-algorithm. While very effective, these methods remain highly tailored to specific problem instances and demand considerable domain expertise, hindering adaptation to new applications and limiting widespread adoption.

We show that it is possible to implement various BM-factorization-based certifiable estimators using the same factor graph-based modeling and optimization methods already used ubiquitously throughout robotics and computer vision. Our framework preserves the same convergence guarantees as existing custom-built certifiable estimation methods but requires significantly less manual effort and fits directly into existing factor graph-based modeling and optimization libraries and workflows. Ultimately, the factor graph paradigm enables users, even those familiar only with local optimization, to develop scalable and certifiable pipelines with minimal additional engineering effort. Shonan Rotation Averaging [35] pioneered this direction by integrating certifiable estimation with factor graph optimization for rotation averaging, though it requires cumbersome conversions between the Stiefel manifold and rotation group and is limited to a single problem class. In contrast, we propose a general certifiable factor graph framework that operates directly on manifold-valued variables, supports a wide range of state estimation tasks, and presents a comprehensive theoretical analysis establishing the connection between quadratically constrained quadratic programs (QCQPs) and their factor graph representations in certifiable estimation via BM factorization.

IV. FACTOR GRAPHS FOR ROBOT PERCEPTION

In this section we briefly review the use of *factor graphs* for modeling and solving statistical estimation problems arising in robotic perception and state estimation tasks. Readers are encouraged to consult the monograph [6] for additional detail.

A. Modeling perception problems with factor graphs

At its core, *perception* is the problem of constructing a model of the world from sensor data. As the measurements produced by real-world sensors are typically noisy, it is standard practice to formulate robotic perception problems as *probabilistic inference* tasks [1].

Robotic perception tasks are typically formalized as follows. Let $X \triangleq (X_1, \dots, X_N)$ denote a collection of N unknown parameters (i.e. the *model*) whose values we would like to infer, and $\tilde{z} \triangleq \{\tilde{z}_k\}_{k=1}^K$ be a set of K available noisy sensor measurements. We assume that each measurement \tilde{z}_k is sampled (conditionally) independently from a probabilistic generative model according to:

$$\tilde{z}_k \sim p_k(\cdot | X_{S_k}) \quad \forall k \in [K], \quad (8)$$

where parameter indices $S_k \subseteq [N]$ specify the *subset* X_{S_k} of the model parameters X on which the k th observation \tilde{z}_k depends. Intuitively, each generative model (8) describes the operation of an individual sensor (i.e., it describes how a given state X_{S_k} of the world gives rise to a distribution $\tilde{z}_k \sim p_k(\cdot | X_{S_k})$ over possible noisy readings \tilde{z}_k that sensor might return).

Let us now make a few simple but important observations about the measurement model (8). First, note that (8) makes explicit the fact that in many real-world applications, each individual measurement \tilde{z}_k typically only depends upon a *small subset* X_{S_k} of the total set of model parameters X (i.e. $|S_k| \ll N$).² Second, the conditional independence of the measurements \tilde{z}_k implies that the joint likelihood $p(\tilde{z}|X)$ of the complete model X given all of the data \tilde{z} factors as the product of the individual measurement likelihoods in (8):

$$p(\tilde{z}|X) = \prod_{k=1}^K p_k(\tilde{z}_k | X_{S_k}). \quad (9)$$

Factor graphs provide a convenient graphical representation for modeling the factorization (9) of the joint likelihood $p(\tilde{z}|X)$. In brief, the factor graph \mathcal{G} (see Figure 1) associated to the factorization (9) is the bipartite graph $\mathcal{G} = (\mathcal{V}, \mathcal{F}, \mathcal{E})$ in which:

- The *variable nodes* $\mathcal{V} \triangleq \{X_1, \dots, X_N\}$ consist of the model parameters to be estimated;
- The *factor nodes* $\mathcal{F} \triangleq \{p_1, \dots, p_K\}$ consist of the individual factors (i.e. measurement likelihoods, conditional distributions) p_k appearing on the right-hand side of (9);
- The *edge set* is defined as:

$$\mathcal{E} \triangleq \{(X_n, p_k) \in \mathcal{V} \times \mathcal{F} \mid X_n \in X_{S_k}\}; \quad (10)$$

²For example, while a visual mapping task may involve the joint estimation of thousands of camera poses and millions of 3D point positions, *each individual observed image feature point* \tilde{z}_k only depends upon *two* of these model parameters: the pose of the individual camera that captured *that specific* point observation, and the 3D position of the imaged point.

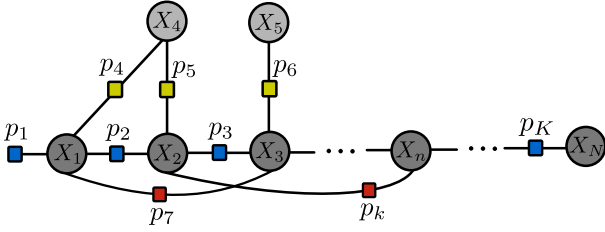


Fig. 1: An example factor graph. This graph models a simple landmark SLAM problem containing N variables X_n and K factors p_k . The variables consist of both *robot poses* (dark gray) and *landmarks* (light gray), while the factors consist of a *unary prior* p_1 on the initial robot pose X_1 , binary *odometry* factors between successive robot poses (blue), *landmark observations* (yellow), and *loop closure* detections (red).

that is, variable X_n and factor p_k are joined by an edge in \mathcal{G} if and only if X_n is an argument of the measurement likelihood p_k in (9).

From a practical standpoint, factor graphs are useful because they provide a simple, general, modular modeling language for constructing complex, high-dimensional joint distributions $p(\tilde{z}|X)$ by composing simple constituent parts [i.e. the individual measurement likelihoods $p_k(\tilde{z}_k|X_{S_k})$ appearing in (8)]. Consequently, several current state-of-the-art software libraries for robotic perception [7]–[9] are based upon this abstraction: when using these libraries, a practitioner specifies a perception task by constructing its associated factor graph model. This simple, object-oriented programming paradigm enables practitioners to easily model a vast array of robotic perception and state estimation tasks by combining standard building blocks, each corresponding to familiar state representations and sensing modalities.

B. Maximum likelihood estimation in factor graphs

Inference in factor graphs is typically performed via *maximum likelihood estimation* (MLE), or more generally *M-estimation* [36]. Recall that in this approach, one determines a point estimate \hat{X}_{MLE} for the unknown parameter X by *maximizing* the value of the likelihood function $p(\tilde{z}|X)$; intuitively, this is the point estimate that “best explains” the available data \tilde{z} . Assuming that the likelihood function $p(\tilde{z}|X)$ factors according to (9), and that the n th parameter X_n takes values in the set \mathcal{X}_n , we may formalize the maximum likelihood estimation task as the following optimization problem:

$$\hat{X}_{\text{MLE}}(\tilde{z}) \triangleq \underset{X_n \in \mathcal{X}_n}{\operatorname{argmin}} \sum_{k=1}^K \ell_k(X_{S_k}; \tilde{z}_k), \quad (11)$$

where the k th summand $\ell_k(X_{S_k}; \tilde{z}_k)$ in (11) is either the negative log-likelihood $-\log p_k(\tilde{z}_k|X_{S_k})$ of the k th conditional distribution p_k in (9), or a robust generalization thereof [36].³

Formulating factor graph inference as the maximum likelihood estimation (11) provides several important advantages. From a theoretical standpoint, maximum likelihood estimation

³While ℓ_k models the *negative log-likelihood* of the factor p_k in (11), in the robotics literature it is common (in a slight abuse of terminology) to also refer to ℓ_k itself as a “factor”, since this is ultimately the function that one actually implements in factor graph-based software libraries (c.f. e.g. [7], [37]) in order to instantiate the MLE (11). We will likewise adopt this convention.

provides strong guarantees on the statistical properties of the resulting estimator \hat{X}_{MLE} , including asymptotic consistency and normality under mild conditions [38]. Computationally, in the typical case that the parameter spaces \mathcal{X}_n are smooth manifolds and the summands ℓ_k are smooth functions, the maximum likelihood estimation (11) is a smooth optimization problem defined over a product of smooth manifolds, enabling us to apply fast sparsity-exploiting first- or second-order smooth optimization methods on manifolds [10], [17], [34] to efficiently recover critical points. This computational efficiency is essential for enabling real-time performance on resource-limited mobile robotic platforms (and indeed several state-of-the-art algorithms based upon this formulation are capable of processing inference problems involving tens to hundreds of thousands of states in real time [8], [11], [12]). Finally, from an operational standpoint, in the typical case in which each parameter set \mathcal{X}_n is a “standard” smooth manifold whose global geometry and topology are known (e.g. common matrix Lie groups, etc.), it is possible to automatically (algorithmically) synthesize and run a fast smooth local optimization algorithm to recover a critical point of the MLE (11) directly from the factor graph model \mathcal{G} describing the inference task.⁴ This capability is a core feature of several notable state-of-the-art software libraries for robotic perception (including GTSAM [37], g2o [8], and Ceres [9]), and is a major factor of their utility, as it enables practitioners to automatically synthesize and deploy highly-efficient inference algorithms directly from a factor-graph specification of the task to be solved, without requiring any specialized knowledge (e.g. of geometry or numerical optimization) or manual algorithm design on the part of the user. The practical impact is that these libraries dramatically reduce the effort necessary to implement and deploy high-performance real-time perception systems, especially for users without extensive subject matter expertise in applied mathematics (e.g. differential geometry, numerical linear algebra, and numerical optimization).

However, despite its many favorable properties, practical implementations of the maximum likelihood estimation (11) often suffer from a lack of *reliability*, due to their reliance upon fast *local* optimization methods. Specifically, these local optimization methods can only guarantee convergence to *stationary points* of (11), rather than the *global minimizer* \hat{X}_{MLE} required in (11). The result is that the inference algorithms employed in common factor graph-based robotic perception libraries can be surprisingly brittle, often returning egregiously wrong estimates even when the problems to which they are applied are well-posed [4]. This lack of reliability motivates the use of the more robust *certifiable* estimation methods we consider in the next section.

V. CERTIFIABLE ESTIMATION

In this section, we briefly review the certifiable estimation pipeline that forms the foundation of our certifiable factor

⁴More precisely: we require that each $\mathcal{X}_n \subseteq \mathbb{R}^{r_n}$ is a smooth embedded submanifold of some Euclidean space \mathbb{R}^{r_n} , and that at each point $x \in \mathcal{X}_n$, we have access to computationally-convenient descriptions of (i) the tangent space $T_x(\mathcal{X}_n)$ of \mathcal{X}_n at x , (ii) the orthogonal projection operator $\Pi_x: \mathbb{R}^{r_n} \rightarrow T_x(\mathcal{X}_n)$ from the ambient space \mathbb{R}^{r_n} to the tangent space $T_x(\mathcal{X}_n) \subseteq \mathbb{R}^{r_n}$ at x , and (iii) a *retraction* operator $R_x: T_x(\mathcal{X}_n) \rightarrow \mathcal{X}_n$ at x [17], [34].

graph approach. Section V-A introduces *Shor's relaxation*, the convex relaxation upon which our certifiable estimators are built. Section V-B describes *Burer-Monteiro factorization*, a computational technique for efficiently solving large-scale semidefinite programs by recasting them as lower-dimensional nonconvex programs, together with a verification procedure for certifying the global optimality of candidate solutions recovered from these lower-dimensional nonlinear programs. Finally, Section V-C presents the *Riemannian Staircase*, a meta-algorithm that integrates these components into a complete procedure for efficiently recovering globally optimal solutions of large-scale SDP relaxations.

A. Shor's relaxation

Many common robotic perception and state estimation tasks have MLEs (11) that naturally take the form of (or can be equivalently recast as) *quadratically-constrained quadratic programs* (QCQPs), i.e., optimization problems in which the objective and constraint functions are all *quadratic*. This class of problems admits a general procedure, called *Shor's relaxation* [39], for constructing strong convex relaxations.

Let us assume that we have an estimation problem in the form of a standard QCQP:

$$\begin{aligned} f_{\text{QCQP}}^* &= \min_{X \in \mathbb{R}^{r \times d}} \langle Q, XX^T \rangle \\ &\text{s.t. } \langle A_m, XX^T \rangle = b_m, \quad m \in [M] \end{aligned} \quad (12)$$

with objective matrix $Q \in \mathbb{S}^r$, constraint matrices $A_m \in \mathbb{S}^r$ for all $m \in [M]$, constraint vector $b \in \mathbb{R}^M$, and $d \leq r$. Note that the decision variable $X \in \mathbb{R}^{r \times d}$ only enters problem (12) through the outer product XX^T , which is a symmetric, positive semidefinite matrix satisfying $\text{rank}(XX^T) \leq d$ by construction.

Shor's relaxation simply consists of replacing the low-rank symmetric outer product XX^T appearing in the QCQP (12) with a *generic* symmetric and positive semidefinite matrix $Z \in \mathbb{S}_+^r$ of the same dimension, producing the following (convex) *semidefinite program* (SDP) relaxation:

$$\begin{aligned} f_{\text{SDP}}^* &= \min_{Z \in \mathbb{S}_+^r} \langle Q, Z \rangle \\ &\text{s.t. } \langle A_m, Z \rangle = b_m, \quad m \in [M]. \end{aligned} \quad (13)$$

While simple to construct, Shor's relaxation (13) turns out to possess many useful properties. First, in marked contrast to the original nonconvex QCQP (12), Shor's relaxation is a *convex program*, from which we can recover a *global* minimizer Z^* in polynomial time using standard interior-point methods [40]. Second, it is easy to see that Shor's relaxation constitutes an *outer approximation* of the original QCQP (12): note that every point X that is feasible for (12) maps to a symmetric outer product XX^T that is also feasible for (13). Intuitively, we can thus regard (13) as being obtained from (12) by *expanding the latter's feasible set*. It immediately follows that the optimal value obtained by minimizing over this enlarged feasible set must *lower bound* the optimal value of (12):

$$f_{\text{SDP}}^* \leq f_{\text{QCQP}}^*. \quad (14)$$

In turn, inequality (14) enables us to easily *upper bound* the suboptimality of *any* feasible point X as a solution of the QCQP (12) according to:

$$\langle Q, XX^T \rangle - f_{\text{QCQP}}^* \leq \langle Q, XX^T \rangle - f_{\text{SDP}}^*. \quad (15)$$

In particular, if the right-hand side of (15) is small, this enables us to conclude that X is a *near-optimal* solution of the QCQP (12) *without* having to directly compute its optimal value f_{QCQP}^* . This observation forms the basis of the *solution verification* mechanism used in certifiable estimators [41].

Finally, suppose that we solve Shor's relaxation (13), and it so happens that the recovered minimizer $Z^* \in \mathbb{S}_+^r$ satisfies $\text{rank}(Z^*) \leq d$. Then Z^* admits a symmetric factorization of the form $Z^* = X^*X^{*\top}$ for some $X^* \in \mathbb{R}^{r \times d}$, and it is straightforward to verify that the low-rank factor X^* so obtained is both feasible for the original QCQP (12) and achieves the same objective value as Z^* . Consequently, it follows [from (15)] that X^* is actually a *globally optimal* solution for the original QCQP (12).⁵

The remarkable fact that justifies our interest in Shor's relaxation (13) is that it is typically *exact* when the original QCQP (12) is an instance of the maximum likelihood estimation (11), provided that the noise on the available data \tilde{z} is not too large [20], [42]. In this favorable case, we can efficiently recover an *exact, certifiably globally optimal* solution of the nonconvex QCQP (i.e., the *correct* maximum likelihood estimate \hat{X}_{MLE}) by solving the (convex) Shor relaxation (13). This algorithmic strategy is the basis of certifiable estimation methods.

B. Solving the semidefinite relaxation

In this section, we describe an effective algorithmic approach for solving large-scale instances of Shor's relaxation (13) efficiently.

1) *Exploiting low-rank structure via Burer-Monteiro factorization*: As a semidefinite program, Shor's relaxation (13) can *in principle* be solved efficiently using general-purpose convex optimization algorithms (such as interior-point methods) [43]; *in practice*, however, the $\mathcal{O}(r^2)$ cost of storing and manipulating the dense symmetric matrix decision variable Z prevents these general-purpose techniques from scaling to problems whose dimension r is greater than a few thousand [14]. Unfortunately, many foundational robotic perception problems (such as SLAM) are often several orders of magnitude larger than this maximum effective problem size, placing them well beyond the reach of these general-purpose techniques.

On the other hand, the *specific instances* of the SDP (13) that we are interested in solving in the context of certifiable estimation exhibit additional useful structure: namely, they generically admit *low rank solutions* Z^* . Indeed, we saw in the previous section that when Shor's relaxation (13) of the QCQP (12) is exact, it admits a rank- d solution of the form $Z^* = X^*X^{*\top}$, where $X^* \in \mathbb{R}^{r \times d}$ is a global minimizer of (12). More generally, a considerable body of prior work has shown that even instances of (13) that are *not* exact still admit solutions Z^* with a rank not much greater than d .

⁵In this case, the relaxation (13) is said to be *exact*.

In their seminal work, Burer and Monteiro [15] proposed an elegant approach for efficiently solving large-scale SDPs that admit such low rank solutions. Suppose that the SDP (13) admits a solution $Z^* \in \mathbb{S}_+^r$ of rank $p^* \triangleq \text{rank}(Z^*)$. Then Z^* can be concisely represented using a symmetric rank factorization of the form $Z^* = Y^*Y^{*\top}$ for some $Y^* \in \mathbb{R}^{r \times p^*}$. Burer and Monteiro proposed to algorithmically exploit this observation by reparameterizing the decision variable Z appearing in (13) using an assumed rank- p factorization of the form $Z = YY^\top$. Substituting this parameterization into Shor's relaxation then produces the following modification of (13), called the *Burer-Monteiro (BM) factorization*:

$$f_{\text{BM}}^* = \min_{Y \in \mathbb{R}^{r \times p}} \langle Q, YY^\top \rangle \quad (16)$$

$$\text{s.t. } \langle A_m, YY^\top \rangle = b_m, \quad m \in [M].$$

The BM factorization (16) affords several important advantages versus the original SDP (13). First, the symmetric matrix decision variable $Z \in \mathbb{S}_+^r$ in (13) requires $\mathcal{O}(r^2)$ storage, while the symmetric rank factor $Y \in \mathbb{R}^{r \times p}$ appearing in (16) requires only $\mathcal{O}(rp)$; in particular, this implies that the latter problem is *much* lower-dimensional than the former when $p \ll r$. Second, note that since $YY^\top \succeq 0$ by construction, it is not necessary to explicitly enforce the positive-semidefiniteness constraint from the original SDP (13) in its BM factorization (16); consequently, the latter takes the form of a standard equality-constrained *nonlinear program* (NLP), rather than a *semidefinite program* that involves both equality and (more complex) conic positive-semidefiniteness constraints. Finally, it is straightforward to verify that if the SDP (13) admits a solution $Z^* \in \mathbb{S}_+^r$ of rank $p^* \triangleq \text{rank}(Z^*)$, then so long as the rank parameter p in (16) is chosen such that $p \geq p^*$, any (global) minimizer $Y^* \in \mathbb{R}^{r \times p}$ of (16) is a symmetric rank factor for a (global) minimizer $Y^*Y^{*\top} \in \mathbb{S}_+^r$ of (13). Consequently, our approach will be to apply standard off-the-shelf (and highly mature, efficient, and scalable) nonlinear programming algorithms and software libraries to the BM factorization (16) in order to search for a low-rank factor Y^* of an optimal solution $Z^* = Y^*Y^{*\top}$ of Shor's relaxation (13).

2) *Verifying global optimality*: While the BM factorization is amenable to fast *local* optimization via standard NLP methods, the quadratic equality constraints appearing in (16) make this problem *nonconvex*; consequently, there is no guarantee that a stationary point $Y^* \in \mathbb{R}^{r \times p}$ recovered from (16) via fast *local* optimization is a *global* minimizer. To address this potential pitfall, in this section we describe how to determine whether a given first-order stationary point $Y^* \in \mathbb{R}^{r \times p}$ of the BM factorization (16) is a low-rank factor for a (global) minimizer $Z^* = Y^*Y^{*\top}$ of Shor's relaxation (13).

In brief, our optimality verification procedure is based upon comparing the first-order Karush-Kuhn-Tucker (KKT) conditions for the BM factorization (16) with those of the original SDP (13). To state these more concisely, let $\mathcal{A} : \mathbb{S}^r \rightarrow \mathbb{R}^M$ denote the linear map defined by:

$$\mathcal{A}(Z)_m \triangleq \langle A_m, Z \rangle \quad \forall m \in [M], \quad (17)$$

$\mathcal{A}^* : \mathbb{R}^M \rightarrow \mathbb{S}^r$ its associated adjoint:

$$\mathcal{A}^*(x) = \sum_{m=1}^M x_m A_m. \quad (18)$$

With these definitions in hand, we may state the KKT conditions for (13) and (16) as follows:

KKT conditions for Shor's relaxation: A point $Z \in \mathbb{S}_+^r$ is a KKT point of (13) if and only if there exists a corresponding Lagrange multiplier $\lambda \in \mathbb{R}^M$ such that the following conditions are satisfied:

$$\mathcal{A}(Z) = b, \quad SZ = 0, \quad S \succeq 0, \quad (19)$$

where $S \in \mathbb{S}^r$ is the symmetric matrix defined by:

$$S \triangleq Q + \mathcal{A}^*(\lambda). \quad (20)$$

KKT conditions for the Burer-Monteiro factorization: A point $Y \in \mathbb{R}^{r \times p}$ is a KKT point of the BM factorization (16) if and only if there exists an associated Lagrange multiplier $\lambda \in \mathbb{R}^M$ such that the following conditions are satisfied:

$$\mathcal{A}(YY^\top) = b, \quad SY = 0, \quad (21)$$

where S is once again as defined in (20).

Comparing (19) and (21), we may deduce the following relation between KKT points of (13) and (16).

Theorem 1 (Theorem 4 of [41]): Suppose that Shor's relaxation (13) satisfies Slater's constraint qualification, and let $Y \in \mathbb{R}^{r \times p}$ be a KKT point of the BM factorization (16) (with corresponding Lagrange multiplier $\lambda \in \mathbb{R}^M$) that satisfies the linear independence constraint qualification. Then exactly one of the following two cases holds:

- $S \succeq 0$ and $Z = YY^\top$ is a global minimizer of (13).
- There exists $v \in \mathbb{R}^r$ such that $v^\top S v < 0$, and in that case, $Y_+ \triangleq (Y \ 0) \in \mathbb{R}^{r \times (p+1)}$ is a KKT point of (16) attaining the same objective value as Y , and $\dot{Y}_+ \triangleq (0 \ v) \in \mathbb{R}^{r \times (p+1)}$ is a feasible second-order direction of descent from Y_+

The practical significance of Theorem 1 is that it provides an algorithmically useful *theorem of the alternative*: under its hypotheses, a given stationary point Y for the BM factorization (16) is either a low-rank factor for a solution $Z = YY^\top$ of the original SDP (13), or we can construct a *second-order direction of descent* \dot{Y}_+ from the embedding Y_+ of Y into a higher-dimensional instance of (16), enabling us to restart local optimization to continue the search for a low-rank factor of a solution of (13).

C. Riemannian Staircase

Theorem 1 immediately suggests a procedure for efficiently recovering low-rank solutions of the SDP (13) by applying standard local nonlinear optimization algorithms to a *sequence* of progressively higher-dimensional instances of the Burer-Monteiro factorization (16); this algorithm, called the *Riemannian Staircase* [16], [44], is summarized as Algorithm 1. In brief, starting at any initial feasible point $Y \in \mathbb{R}^{r \times p}$ for the p -dimensional instance of (16), we apply *local* optimization to recover a KKT point $Y^* \in \mathbb{R}^{r \times p}$ and its associated Lagrange

Algorithm 1 The Riemannian Staircase

Input: Initial feasible point $Y \in \mathbb{R}^{r \times p}$ for p -dimensional instance of the Burer-Monteiro factorization (16).
Output: Symmetric factor Y^* for a minimizer $Z^* = Y^*Y^{*\top}$ of SDP (13), optimal value f_{SDP}^* .

```

1: function RIEMANNIANSTAIRCASE( $Y$ )
2:   loop
3:     // Find first-order KKT point of (16).
4:      $(Y^*, \lambda^*) \leftarrow \text{LOCALOPTIMIZATION}(Y)$ .
5:     Construct certificate matrix  $S$  from  $\lambda^*$  as in (20).
6:      $(\lambda_{\min}, v_{\min}) \leftarrow \text{MINIMUMEIGENPAIR}(S)$ .
7:     // Test optimality of  $Z^* = Y^*Y^{*\top}$  for (13).
8:     if  $\lambda_{\min} \geq 0$  then
9:       //  $Z^* = Y^*Y^{*\top}$  minimizes (13) by Thm. 1(a).
10:       $f_{\text{SDP}}^* \leftarrow \langle Q, Y^*Y^{*\top} \rangle$ .
11:      return  $\{Y^*, f_{\text{SDP}}^*\}$ 
12:     end if
13:     // Construct lifted embedding of  $Y^*$ .
14:      $Y_+ \leftarrow (Y^* \ 0)$ 
15:     // Construct second-order descent direction.
16:      $\dot{Y}_+ \leftarrow (0 \ v_{\min})$ 
17:     // Backtracking line search for saddle escape.
18:      $Y \leftarrow \text{LINESEARCH}(Y_+, \dot{Y}_+)$ 
19:   end loop
20: end function

```

multiplier $\lambda^* \in \mathbb{R}^M$. Given this stationary point, we then simply check [using the test prescribed in Theorem 1(a)] whether Y^* is a low-rank factor for a solution $Z^* = Y^*Y^{*\top}$ of the SDP (13): if so, we return Y^* , together with the optimal value f_{SDP}^* of the SDP; otherwise, we increase the dimension p of the BM factorization (16), and then invoke Theorem 1(b) to construct a *second*-order direction of descent from the current estimate, enabling us to continue the search (via local optimization) for an optimal low-rank factor.

Remark 1 (Feasibility in local optimization in the Riemannian Staircase): For simplicity of presentation, the formulation of the Riemannian Staircase displayed in Algorithm 1 implicitly assumes that the local optimization in line 3 always returns a feasible point for the BM-factored SDP (16). This assumption is justified whenever the feasible set for (16) turns out to be a smooth manifold, since this admits the use of specialized (smooth manifold-based) optimization algorithms that directly enforce feasibility throughout by construction [17], [34]. This is the case for the majority of previous applications of the Riemannian Staircase methodology in the certifiable estimation literature (cf. e.g. [31] and the references therein), and is consistent with our usage of it in the example applications that we consider in Section VIII. We note, however, that more general formulations of the Riemannian Staircase exist that admit the use of standard (extrinsic) constrained nonlinear programming techniques, which are *not* guaranteed to recover a feasible point in all cases [41]. All of the results presented in this paper extend immediately to this more general setting, provided that the corresponding generalization of Algorithm 1 (cf. Algorithm 1 of [41]) is employed.

VI. CERTIFIABLE FACTOR GRAPH OPTIMIZATION

In this section, we show how the factor graph and certifiable estimation paradigms described in Sections IV and V can be naturally synthesized into a unified framework for *certifiable factor graph optimization*. The key discovery enabling this synthesis is that factor graph structure is *preserved* under Shor’s relaxation and Burer-Monteiro factorization: given an initial QCQP with a nontrivial factor graph representation, we show that the Burer-Monteiro factorization of the associated Shor relaxation admits a factor graph representation with *identical* connectivity, and in which the variables and factors are simple one-to-one algebraic transformations (*lifts*) of the variables and factors appearing in the original QCQP’s factor graph. This result implies that the local optimizations required in each level of the Riemannian Staircase can be instantiated and run using current state-of-the-art factor graph optimization libraries, augmented with these lifted (i.e. *certifiable*) variable and factor types. The practical consequence is that our framework enables practitioners to easily design and deploy certifiable estimators using existing state-of-the-art factor graph-based libraries and workflows, dramatically lowering the barrier to entry and democratizing access to this powerful class of estimation methods.

A. Factor graph structure in QCQPs

We begin the development of our certifiable factor graph framework by studying the natural setting for this synthesis: estimation problems that simultaneously admit a QCQP representation of the form (12) and a nontrivial factor graph representation of the form (11). Our goal is to elucidate how these two structures relate to each other. Our main result is that there is a precise correspondence between the structure of the factor graph and specific block sparsity and separability patterns in the data matrices defining the QCQP (12).

1) *Factor graph structure implies block sparsity and separability in QCQP data matrices:* Consider a maximum likelihood estimation problem in the form of a QCQP (12), and suppose that the decision variable $X \in \mathbb{R}^{r \times d}$ is partitioned into N block rows:

$$X = \begin{bmatrix} X_1 \\ \vdots \\ X_N \end{bmatrix} \quad (22)$$

(with $X_n \in \mathbb{R}^{r_n \times d}$ for all $n \in [N]$ and $r = \sum_{n=1}^N r_n$) such that the resulting MLE admits a factor graph model of the form $\mathcal{G} = (\mathcal{V}, \mathcal{F}, \mathcal{E})$, where:

$$\mathcal{V} \triangleq \{X_1, \dots, X_N\}, \quad (23a)$$

$$\mathcal{F} \triangleq \{\ell_1, \dots, \ell_K\}, \quad (23b)$$

$$\mathcal{E} \triangleq \{(X_n, \ell_k) \in \mathcal{V} \times \mathcal{F} \mid n \in S_k\}. \quad (23c)$$

Note that here the factors ℓ_k are the (generalized) negative log-likelihoods defined in (11), and $S_k \subseteq [N]$ is the set of indices of the variables X_1, \dots, X_N that factor ℓ_k depends upon for all $k \in [K]$. We will show that the structure (23) of the factor graph \mathcal{G} imposes specific block sparsity and separability patterns on the data matrices determining the QCQP (12).

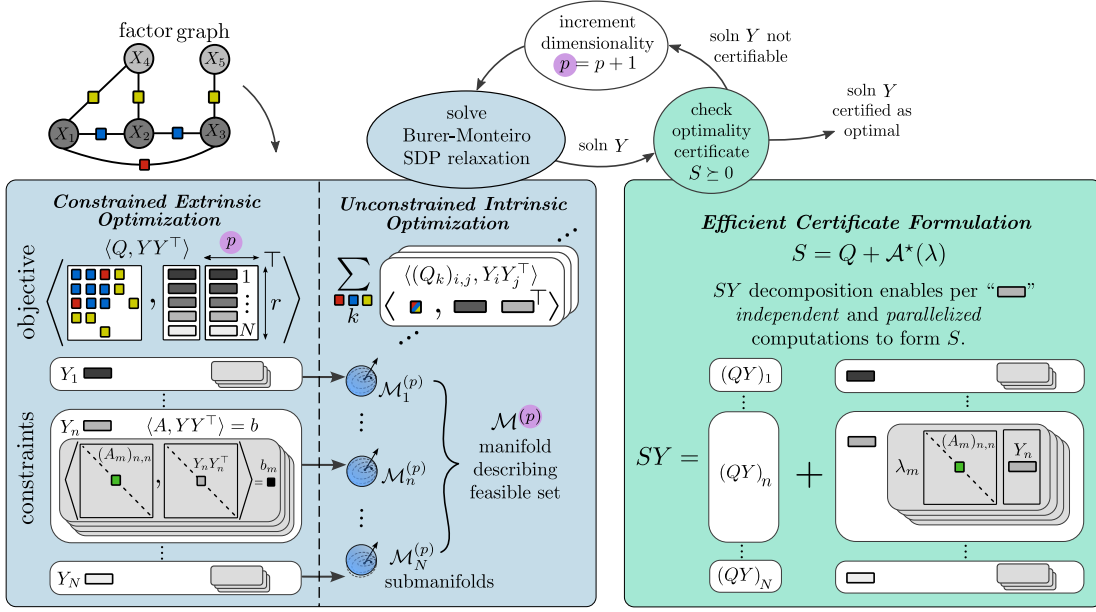


Fig. 2: Overview of our framework for certifiable factor graph optimization. Our approach accepts as input a factor graph model of a QCQP-representable estimation task, and constructs its corresponding rank- p BM-factored Shor relaxation (left). This BM-factored SDP naturally preserves the original QCQP’s factor graph structure, as reflected in the block sparsity pattern of the objective matrix Q and the separable block-diagonal structure of the constraint matrices A_m . Consequently, the constraints on each block variable Y_n in the resulting BM-factored SDP determine a feasible set $\mathcal{M}^{(p)}$ with the structure of a Cartesian product; this enables transformation of the (constrained) BM-factored SDP to an *unconstrained* intrinsic form with two key benefits: (1) automatic problem formulation directly from the (lifted) factor graph structure, and (2) efficient local optimization via smooth manifold-based optimization methods. Following the Riemannian staircase procedure (top), solutions are recovered via a sequence of *local* optimizations over lifted factor graphs, interleaved with certification steps. For constructing the optimality certificate S (right), the block-separable structure of the constraints enables decomposition into N *independent* computations that can be solved efficiently in parallel.

To see this, let us first consider the objective of the MLE [cf. (11)]. Under the stated hypotheses, each factor ℓ_k in (23b) is a quadratic function of the form:

$$\ell_k(X) \triangleq \langle Q_k, XX^T \rangle \quad (24)$$

for some $Q_k \in \mathbb{S}^r$. Partitioning Q_k conformally with (22):

$$Q_k = \begin{bmatrix} (Q_k)_{1,1} & \cdots & (Q_k)_{1,N} \\ \vdots & \ddots & \vdots \\ (Q_k)_{N,1} & \cdots & (Q_k)_{N,N} \end{bmatrix} \quad (25)$$

(where $(Q_k)_{i,j} \in \mathbb{R}^{r_i \times r_j}$ for all $i, j \in [N]$), we may substitute the block decompositions (22) and (25) into (24) to derive:

$$\ell_k(X) = \sum_{i,j=1}^N \langle (Q_k)_{i,j}, X_i X_j^T \rangle. \quad (26)$$

Equation (26) and the symmetry of Q_k imply that factor ℓ_k depends upon variable X_n if and only if there exists some $i \in [N]$ such that $(Q_k)_{n,i} \neq 0$. Equivalently:

$$n \notin S_k \implies (Q_k)_{n,i} = 0 \text{ for all } i \in [N]. \quad (27)$$

That is: if variable X_n is *not* adjacent to factor ℓ_k in \mathcal{G} , then the n th block row and column of Q_k are both *identically zero*. Thus, \mathcal{G} ’s edge set \mathcal{E} (23c) determines a specific block sparsity pattern (27) that the data matrix Q_k parameterizing the k th factor ℓ_k [via (24)] must satisfy.

Similarly, let us now consider the data matrices A_m determining the feasible set in (12). Recall that, by construction,

the feasible set for the MLE determined by the factor graph \mathcal{G} [cf. (11)] is a *Cartesian product*:

$$\mathcal{X} = \mathcal{X}_1 \times \cdots \times \mathcal{X}_N; \quad (28)$$

i.e., each of the variables $X_n \in \mathcal{X}_n$ can be varied within its domain \mathcal{X}_n *independently* of all others. But this immediately implies that the quadratic constraints in (12) must be *separable* over the variables X_1, \dots, X_N .⁶ Consequently, we may partition the index set $[M]$ for the constraints into N subsets L_1, \dots, L_N , where each $L_n \subseteq [M]$ contains the indices of the constraints in (12) associated with variable X_n . Moreover, given any $m \in L_n$, the argument used to derive (24)–(27) implies that if A_m is partitioned conformally with the block decomposition (22), then $(A_m)_{i,j} = 0$ for all $(i, j) \neq (n, n)$; i.e., A_m has only a *single nonzero block*, which must appear on the main block diagonal in the (n, n) -th position:

$$m \in L_n \implies A_m = \begin{bmatrix} 0 & & & & \\ & \ddots & & & \\ & & (A_m)_{n,n} & & \\ & & & \ddots & \\ & & & & 0 \end{bmatrix}. \quad (29)$$

It follows that the constraints in (12) can be written more concisely as:

$$\langle (A_m)_{n,n}, X_n X_n^T \rangle = b_m, \quad \forall m \in L_n, n \in [N]. \quad (30)$$

⁶Note that if any constraint appearing in (12) involved more than one variable (say X_i and X_j for $i \neq j$), this would induce a nontrivial coupling between X_i and X_j that would violate their independence in (28).

In particular, the domain \mathcal{X}_n for the variable X_n is the algebraic variety determined by the constraints indexed by L_n :

$$\mathcal{X}_n = \{X_n \in \mathbb{R}^{r_n \times d} \mid \langle (A_m)_{n,n}, X_n X_n^\top \rangle = b_m \forall m \in L_n\}. \quad (31)$$

Taken together, these observations show that the structure of the factor graph \mathcal{G} defined in (23) implies that the QCQP (12) must decompose into the following block form:

$$\begin{aligned} \min_{X_n \in \mathbb{R}^{r_n \times d}} \sum_{k=1}^K \overbrace{\sum_{(i,j) \in S_k \times S_k} \langle (Q_k)_{i,j}, X_i X_j^\top \rangle}^{\ell_k(X_{S_k})} \quad (32) \\ \text{s.t. } \langle (A_m)_{n,n}, X_n, X_n^\top \rangle = b_m, \forall m \in L_n, n \in [N]. \end{aligned}$$

2) *Block sparsity and separability in QCQP data matrices implies factor graph structure*: Conversely, consider a QCQP of the form (12), and suppose that there exists a row partition (22) of the decision variable X such that (12) admits a sparse block decomposition of the form (32) with respect to the variables X_1, \dots, X_N . We will show that the bipartite graph $\mathcal{G} = (\mathcal{V}, \mathcal{F}, \mathcal{E})$ defined by (23) is a valid factor graph representation of the QCQP (32).

The argument proceeds by simply reversing the logic of Section VI-A1. Since the constraints in (32) are (by construction) separable over X_1, \dots, X_N , the feasible set \mathcal{X} of (32) takes the form of the Cartesian product shown in (28), where the domain \mathcal{X}_n of the n th variable X_n is given by (31). Consequently, the set \mathcal{V} defined in (23a) is a valid variable set for a factor graph model of (32). Similarly, the factor set \mathcal{F} defined in (23b) is (by construction) in one-to-one correspondence with the quadratic summands labeled ℓ_k in the objective of (32), as required. Finally, it is immediate [by inspection of the objective in (32)] that factor ℓ_k only depends upon those variables X_n for which $n \in S_k$; consequently, defining the edge set \mathcal{E} as in (23c) ensures that each factor ℓ_k is adjacent to every variable X_n upon which it explicitly depends. It follows that the bipartite graph $\mathcal{G} = (\mathcal{V}, \mathcal{F}, \mathcal{E})$ determined by (23) provides a valid factor graph model of the QCQP (32), as claimed.

B. Shor relaxation and Burer-Monteiro factorization preserve factor graph structure

In this subsection, we study how the factor graph structure of a QCQP propagates through the certifiable estimation pipeline described in Section V (Shor's relaxation followed by Burer-Monteiro factorization). Our main result is that this structure is in fact *preserved*: the resulting BM-factored Shor relaxation admits a factor graph model that can be obtained by applying simple algebraic transformations (*lifts*) to the individual variables and factors appearing in the original QCQP's factor graph.

The key observation underpinning our proof is that *the same data matrices Q and A_m parameterize both the original QCQP (12) and its Burer-Monteiro-factored Shor relaxation* [cf. equations (12) and (16)].

Since the same data matrices parameterize both problems, it follows that any block sparsity and separability structure implied by a factor graph model of the original QCQP is

automatically inherited by its associated BM-factored Shor relaxation. To see this explicitly, suppose that the QCQP (12) admits the factor graph model $\mathcal{G} = (\mathcal{V}, \mathcal{F}, \mathcal{E})$ defined in (23). The results of Section VI-A1 then imply that the data matrices Q_k and A_m parameterizing this QCQP must exhibit the block sparsity patterns shown in (25) and (29) (respectively), leading to the sparse block decomposition shown in (32). Partitioning the rows of the decision variable Y in (16) conformally with those of X in (22):

$$Y = \begin{bmatrix} Y_1 \\ \vdots \\ Y_N \end{bmatrix}, \quad (33)$$

it follows that the BM-factored Shor relaxation (16) admits the analogous sparse block decomposition:

$$\begin{aligned} \min_{Y_n \in \mathbb{R}^{r_n \times p}} \sum_{k=1}^K \overbrace{\sum_{(i,j) \in S_k \times S_k} \langle (Q_k)_{i,j}, Y_i Y_j^\top \rangle}^{\triangleq \bar{\ell}_k(Y_{S_k})} \quad (34) \\ \text{s.t. } \langle (A_m)_{n,n}, Y_n, Y_n^\top \rangle = b_m, \forall m \in L_n, n \in [N]. \end{aligned}$$

Finally, since the BM-factored Shor relaxation (34) is itself a QCQP, we may apply the argument of Section VI-A2 to construct an associated factor graph $\bar{\mathcal{G}} = (\bar{\mathcal{V}}, \bar{\mathcal{F}}, \bar{\mathcal{E}})$, where:

$$\bar{\mathcal{V}} \triangleq \{Y_1, \dots, Y_N\}, \quad (35a)$$

$$\bar{\mathcal{F}} \triangleq \{\bar{\ell}_1, \dots, \bar{\ell}_K\}, \quad (35b)$$

$$\bar{\mathcal{E}} \triangleq \{(Y_n, \bar{\ell}_k) \in \bar{\mathcal{V}} \times \bar{\mathcal{F}} \mid n \in S_k\}, \quad (35c)$$

and the domain \mathcal{Y}_n of the n th block variable Y_n is the algebraic variety defined by:

$$\mathcal{Y}_n = \{Y_n \in \mathbb{R}^{r_n \times p} \mid \langle (A_m)_{n,n}, Y_n Y_n^\top \rangle = b_m \forall m \in L_n\}. \quad (36)$$

Comparing the factor graph models \mathcal{G} and $\bar{\mathcal{G}}$ determined by (23) and (35) reveals a precise structural correspondence: the variable and factor sets for these two graphs are in one-to-one correspondence, and their connectivities *coincide*. Indeed, comparing the definitions of the feasible sets \mathcal{X}_n and \mathcal{Y}_n in (31) and (36) and the factors ℓ_k and $\bar{\ell}_k$ in (32) and (34) (respectively) reveals that the variables and factors appearing in $\bar{\mathcal{G}}$ can be viewed as *higher-dimensional analogues* of those appearing in \mathcal{G} , and that the former are obtained from the latter by means of simple and explicit algebraic transformations (*lifts*). We refer to these higher-dimensional variable and factor types as *lifted* or *certifiable* variables and factors.

The practical significance of the preceding analysis is that if we are given a factor graph model \mathcal{G} for a QCQP of the form (12), we can obtain a factor graph model $\bar{\mathcal{G}}$ for its associated BM-factored Shor relaxation (16) simply by replacing the individual variables and factors appearing in \mathcal{G} with their lifted counterparts. In particular, this means that we can easily implement the low-dimensional *local* optimizations required in the Riemannian Staircase (Alg. 1) using current state-of-the-art factor graph-based modeling and optimization libraries, provided that they have been augmented with the requisite certifiable variable and factor types.

C. Block separability enables efficient certificate computation

In this subsection, we show that the block separability of the constraints in the BM-factored Shor relaxation (34) implied by the factor graph structure $\bar{\mathcal{G}}$ in (35) can also be exploited to improve the computational efficiency of constructing the certificate matrix S (20) employed in the optimality verification test in the Riemannian Staircase (Alg. 1).

The key insight enabling this result is that the block separability of the constraints in (34) induces a corresponding block-diagonal structure in the adjoint operator \mathcal{A}^* defined in (18). Specifically, recalling the partition $L_1, \dots, L_N \subseteq [M]$ of the constraints in (34) and the induced block-sparsity pattern (29) in the corresponding constraint data matrices A_m , we may express the adjoint operator \mathcal{A}^* more explicitly as:

$$\begin{aligned} \mathcal{A}^*(\lambda) &= \sum_{m=1}^M \lambda_m A_m = \sum_{n=1}^N \sum_{m \in L_n} \lambda_m A_m \\ &= \begin{bmatrix} \sum_{m \in L_1} \lambda_m (A_m)_{1,1} & & \\ & \ddots & \\ & & \sum_{m \in L_N} \lambda_m (A_m)_{N,N} \end{bmatrix}. \end{aligned} \quad (37)$$

Equation (37) reveals that $\mathcal{A}^*(\lambda)$ takes the form of a block-diagonal matrix in which the n th diagonal block is constructed using *only* the constraint matrices A_m and Lagrange multipliers λ_m associated with the n th variable Y_n . In particular, each of these N diagonal blocks can be constructed independently and in parallel, enabling the certificate matrix $S = Q + \mathcal{A}^*(\lambda)$ to be assembled efficiently.

Moreover, the block-diagonal structure of $\mathcal{A}^*(\lambda)$ also enables the efficient parallel computation of the Lagrange multipliers $\lambda \in \mathbb{R}^M$ themselves. To see this, note that given a feasible (but not necessarily optimal) point $Y \in \mathbb{R}^{r \times p}$ of the BM-factored Shor relaxation (16), one can calculate a corresponding set of optimal *Lagrange multiplier estimates* $\lambda_{LS}^* \in \mathbb{R}^M$ by choosing them to minimize the norm of the stationarity residual in the KKT conditions (21):

$$\begin{aligned} \lambda_{LS}^* &= \operatorname{argmin}_{\lambda \in \mathbb{R}^M} \|S(\lambda)Y\|^2 \\ &= \operatorname{argmin}_{\lambda \in \mathbb{R}^M} \|[Q + \mathcal{A}^*(\lambda)]Y\|^2. \end{aligned} \quad (38)$$

The estimates λ_{LS}^* so obtained are referred to as *least squares Lagrange multiplier estimates*.⁷ Recalling the block decompositions (33) and (37), we may expand (38) as:

$$\begin{aligned} \lambda_{LS}^* &= \operatorname{argmin}_{\lambda \in \mathbb{R}^M} \left\| \begin{bmatrix} (QY)_1 \\ \vdots \\ (QY)_N \end{bmatrix} + \begin{bmatrix} \sum_{m \in L_1} \lambda_m (A_m)_{1,1} Y_1 \\ \vdots \\ \sum_{m \in L_N} \lambda_m (A_m)_{N,N} Y_N \end{bmatrix} \right\|^2 \\ &= \operatorname{argmin}_{\lambda \in \mathbb{R}^M} \sum_{n=1}^N \left\| (QY)_n + \sum_{m \in L_n} \lambda_m (A_m)_{n,n} Y_n \right\|^2. \end{aligned} \quad (39)$$

⁷Note that these estimates are unique (i.e. the right-hand side of (38) admits a unique minimizer) whenever the linear independence constraint qualification is satisfied at Y ; moreover, in that case, the optimal value of the minimization in (38) is 0 if and only if Y is a first-order stationary point of (16), in which case the λ_{LS}^* are the associated Lagrange multipliers *certifying* this fact.

Algorithm 2 The Riemannian Staircase over factor graphs

Input: Initial feasible point $Y = (Y_1, \dots, Y_N) \in \mathbb{R}^{r \times p}$ for p -dimensional BM-factored Shor relaxation (34).

Output: Symmetric factor $Y^* = (Y_1^*, \dots, Y_N^*)$ for minimizer $Z^* = Y^* Y^{*\top}$ of Shor relaxation, optimal value f_{SDP}^* .

```

1: function RIEMANNIANSTAIRCASE( $Y$ )
2:   loop
3:     // Find first-order KKT point of (34).
4:     Construct lifted factor graph model  $\bar{\mathcal{G}} = (\bar{V}, \bar{\mathcal{F}}, \bar{E})$ 
       for rank- $p$  BM factorization via (34)–(36).
5:      $Y^* \leftarrow$  FACTORGRAPHOPTIMIZATION( $\bar{\mathcal{G}}, Y$ ).
6:     Compute Lagrange multipliers  $\lambda^* \in \mathbb{R}^M$  via (40).
7:     Construct certificate  $S$  from  $\lambda^*$  via (20) and (37).
8:      $(\lambda_{\min}, v_{\min}) \leftarrow$  MINIMUMEIGENPAIR( $S$ ).
9:     // Test optimality of  $Z^* = Y^* Y^{*\top}$  for SDP.
10:    if  $\lambda_{\min} \geq 0$  then
11:      //  $Z^* = Y^* Y^{*\top}$  minimizes SDP by Thm. 1(a).
12:       $f_{\text{SDP}}^* \leftarrow \langle Q, Y^* Y^{*\top} \rangle$ .
13:      return  $\{Y^*, f_{\text{SDP}}^*\}$ 
14:    end if
15:    // Construct lifted embedding of  $Y^*$ .
16:     $Y_+ \leftarrow (Y^* \ 0)$ 
17:    // Construct second-order descent direction.
18:     $\dot{Y}_+ \leftarrow (0 \ v_{\min})$ 
19:    // Backtracking line search for saddle escape.
20:     $Y \leftarrow$  LINESEARCH( $Y_+, \dot{Y}_+$ )
21:  end loop
22: end function

```

Note that since the sets L_n *partition* the set of constraint indices $[M]$ (by construction), the multipliers λ_{L_n} associated with the n th variable Y_n appear *only* in the n th summand in the final line of (39); that is, the minimization (39) is *separable* over the multipliers λ_{L_n} . Consequently, we can recover these Lagrange multiplier estimates by solving N *independent* (and *low-dimensional*) linear least-squares problems in parallel:

$$\lambda_{L_n}^* = \operatorname{argmin}_{\lambda_{L_n} \in \mathbb{R}^{|L_n|}} \left\| (QY)_n + \sum_{m \in L_n} \lambda_m (A_m)_{n,n} Y_n \right\|^2. \quad (40)$$

D. The Riemannian Staircase over factor graphs

The results of Sections VI-A–VI-C together enable the Riemannian Staircase to be easily implemented and deployed using the same mature, highly-performant factor graph libraries and associated workflows already ubiquitously employed throughout robotics and computer vision. This factor graph-based instantiation of the Riemannian Staircase is summarized as Algorithm 2.

Note that Algorithm 2 is simply a concrete realization of the generic Riemannian Staircase (Algorithm 1) that makes explicit how several of the required (abstract) operations (namely local optimization, Lagrange multiplier computation, and certificate matrix construction) can be efficiently implemented within the factor graph paradigm. Specifically, in Algorithm 2 the local optimization required at each level of the Riemannian

Staircase (line 3 of Algorithm 1) is carried out in line 4 as a standard factor graph optimization over the rank- p lifted factor graph $\tilde{\mathcal{G}} = (\tilde{\mathcal{V}}, \tilde{\mathcal{F}}, \tilde{\mathcal{E}})$, which can be automatically synthesized directly from the factor graph model $\mathcal{G} = (\mathcal{V}, \mathcal{F}, \mathcal{E})$ specifying the original QCQP estimation task using the constructive lifting (i.e. one-to-one variable and factor substitution) procedure described in Section VI-B. Given the first-order stationary point Y^* recovered from this factor graph optimization, an associated set of optimal Lagrange multipliers λ^* can then be computed efficiently (in line 5) via the N independent low-dimensional linear least-squares solves described in Section VI-C.⁸ Finally, the N diagonal blocks of the adjoint operator $\mathcal{A}^*(\lambda^*)$ required to construct the certificate matrix S in (20) can then be assembled independently and in parallel (in line 6) as shown in (37). Crucially, both of the latter two operations (Lagrange multiplier computation and adjoint operator evaluation) are *separable* over the individual variables Y_n , and the contribution associated with each variable Y_n depends only upon its own value and the quadratic equations defining its domain \mathcal{Y}_n in (36). This separability is in keeping with the modular design philosophy of the factor graph paradigm; in particular, at the level of software, these computations can be implemented as *member functions* within the classes defining the domains \mathcal{Y}_n of the lifted variables Y_n appearing in the lifted factor graph $\tilde{\mathcal{G}}$.

Finally, we note that the synthesis of the factor graph and certifiable estimation paradigms developed in this section (and instantiated in Algorithm 2) is mutually beneficial. From the perspective of certifiable estimation, our synthesis dramatically lowers the practical barriers to designing and deploying certifiable estimators: practitioners can now obtain verifiably globally optimal solutions using existing factor graph libraries and workflows, with no specialized expertise in convex optimization or semidefinite programming and no custom solver development required. In short, certifiable estimation becomes as straightforward to implement and deploy as conventional local factor graph optimization. From the perspective of factor graph inference, the Riemannian Staircase (Algorithm 2) can be viewed as a lightweight meta-algorithm that wraps around standard *local* factor graph optimization, yet is capable of guaranteeing the recovery of *certifiably globally optimal solutions*. Our synthesis thus achieves the best of both worlds: it combines the robustness and formal global optimality guarantees of certifiable estimation with the simplicity, ease of use, and high computational performance of current state-of-the-art factor graph-based modeling and optimization libraries.

VII. COMMON EXAMPLES OF LIFTED VARIABLES AND FACTORS FOR CERTIFIABLE FACTOR GRAPH OPTIMIZATION

In this section, we present the *lifted* analogues of several variable and factor types commonly encountered in robotics

⁸This efficient computation of Lagrange multiplier estimates is particularly important when the factor graph optimizations in line 4 are implemented using manifold-based optimization algorithms (such as those employed in e.g. GTSAM [37] or Manopt [45]): since these methods are *intrinsic* (i.e., they formulate the problem as *unconstrained* optimization over a smooth manifold), they do not natively return an associated set of Lagrange multipliers.

and computer vision. These data types provide the concrete building blocks necessary to implement the experimental evaluations reported in Section VIII.

A. Common lifted variable types

1) *Rotations and orthogonal matrices*: Following [20], we model both rotations $R \in \text{SO}(d)$ and orthogonal matrices $R \in \text{O}(d)$ as elements of the orthogonal group by enforcing the orthonormality constraints:

$$R^T R = I_d. \quad (41)$$

Following Section VI-B, the lifted variable $Y \in \mathbb{R}^{p \times d}$ corresponding to $R \in \mathbb{R}^{d \times d}$ satisfies the constraints [cf. (36)]:

$$Y^T Y = I_d, \quad (42)$$

which we may recognize as the defining equations for the Stiefel manifold $\text{St}(d, p)$.

2) *Unit vectors*: We model unit vectors $v \in S^{d-1}$ in d -dimensional Euclidean space with the constraint:

$$v^T v = 1. \quad (43)$$

The lifted variable $u \in \mathbb{R}^p$ corresponding to $v \in \mathbb{R}^d$ likewise satisfies the constraint:

$$u^T u = 1, \quad (44)$$

which we recognize as the defining equation for the (higher-dimensional) unit sphere S^{p-1} in p -dimensional Euclidean space.

3) *Translations*: Translation variables $t \in \mathbb{R}^d$ are *unconstrained*, i.e., the set of quadratic equations appearing on the right-hand side of (36) is empty. Consequently, a d -dimensional translation t simply lifts to the higher-dimensional translation $u \in \mathbb{R}^p$.

B. Common lifted factor types

1) *Relative rotation measurements*: Given two rotations $R_i, R_j \in \text{SO}(d)$, the *relative rotation* $R_{ij} \in \text{SO}(d)$ from R_i to R_j is:

$$R_{ij} \triangleq R_i^{-1} R_j. \quad (45)$$

Following [20], we assume that noisy relative rotation measurements $\tilde{R}_{ij} \in \text{SO}(d)$ are sampled according to:

$$\tilde{R}_{ij} = R_{ij} \eta_{ij}, \quad \eta_{ij} \sim \text{Langevin}(I_d, \kappa_{ij}), \quad (46)$$

where $\text{Langevin}(I_d, \kappa_{ij})$ denotes the *isotropic Langevin distribution* over $\text{SO}(d)$ with concentration parameter $\kappa_{ij} \geq 0$. The negative log-likelihood function corresponding to the measurement model (45)–(46) is then:

$$\ell(R_i, R_j; \tilde{R}_{ij}) = \kappa_{ij} \|R_j - R_i \tilde{R}_{ij}\|_F^2. \quad (47)$$

Following Section VI-B, the *lifted* relative rotation factor corresponding to (47) is:

$$\tilde{\ell}(Y_i, Y_j; \tilde{R}_{ij}) = \kappa_{ij} \|Y_j - Y_i \tilde{R}_{ij}\|_F^2. \quad (48)$$

2) *Relative translation measurements*: Given a point $t_j \in \mathbb{R}^d$ and a pose $x_i = (t_i, R_i) \in \text{SE}(d)$, the *relative translation* $t_{ij} \in \mathbb{R}^d$ from x_i to t_j (as measured from the coordinate frame defined by x_i itself) is:

$$t_{ij} \triangleq R_i^{-1}(t_j - t_i). \quad (49)$$

We assume that noisy relative translation measurements $\tilde{t}_{ij} \in \mathbb{R}^d$ are sampled according to:

$$\tilde{t}_{ij} = t_{ij} + \epsilon_{ij}, \quad \epsilon_{ij} \sim \mathcal{N}(0, \tau_{ij}^{-1} I_d), \quad (50)$$

where $\tau_{ij} \geq 0$ denotes the measurement precision. The negative log-likelihood function corresponding to the measurement model (49)–(50) is then:

$$\ell(R_i, t_i, t_j; \tilde{t}_{ij}) = \tau_{ij} \|t_j - t_i - R_i \tilde{t}_{ij}\|_2^2. \quad (51)$$

Following Section VI-B, the *lifted* relative translation factor corresponding to (51) is:

$$\bar{\ell}(Y_i, u_i, u_j; \tilde{t}_{ij}) = \tau_{ij} \|u_j - u_i - Y_i \tilde{t}_{ij}\|_2^2. \quad (52)$$

3) *Range measurements*: Given two points $t_i, t_j \in \mathbb{R}^d$, the *range* $r_{ij} \in \mathbb{R}_+$ between them is:

$$r_{ij} \triangleq \|t_i - t_j\|_2. \quad (53)$$

We assume that noisy range measurements are sampled according to:

$$\tilde{r}_{ij} = r_{ij} + \nu_{ij}, \quad \nu_{ij} \sim \mathcal{N}(0, \sigma_{ij}^2), \quad (54)$$

where σ_{ij}^2 is the measurement variance. The negative log-likelihood function corresponding to (53)–(54) is then:

$$\ell(t_i, t_j; \tilde{r}_{ij}) = \frac{1}{\sigma_{ij}^2} (\|t_j - t_i\|_2 - \tilde{r}_{ij})^2. \quad (55)$$

Note that (55) is *not* a quadratic function of t_i and t_j , due to the unsquared norm appearing on the right-hand side. Following [31], [46], we introduce an auxiliary variable $b_{ij} \in S^{d-1}$ associated with this measurement that represents the *bearing* from t_i to t_j , which can be shown to yield an *equivalent* quadratic formulation:

$$\ell(t_i, t_j, b_{ij}; \tilde{r}_{ij}) = \frac{1}{\sigma_{ij}^2} \|t_j - t_i - \tilde{r}_{ij} b_{ij}\|_2^2. \quad (56)$$

Following Section VI-B, the *lifted* range factor corresponding to (56) is:

$$\bar{\ell}(u_i, u_j, s_{ij}; \tilde{r}_{ij}) = \frac{1}{\sigma_{ij}^2} \|u_j - u_i - \tilde{r}_{ij} s_{ij}\|_2^2. \quad (57)$$

C. Summary

For ease of reference, we summarize the lifted variable and factor types described in this section in Table I. These lifted types can be composed to formulate a wide variety of certifiable estimators, as demonstrated in our experimental evaluations (Section VIII).

TABLE I
Summary of common lifted variable and factor types

Type	Original	Lifted (rank- p)
Rotation	$R \in O(d)$	$Y \in \text{St}(d, p)$
Unit sphere	$v \in S^{d-1}$	$u \in S^{p-1}$
Translation	$t \in \mathbb{R}^d$	$u \in \mathbb{R}^p$
Relative rotation	$\kappa_{ij} \ R_j - R_i \tilde{R}_{ij}\ _F^2$	$\kappa_{ij} \ Y_j - Y_i \tilde{R}_{ij}\ _F^2$
Relative translation	$\tau_{ij} \ t_j - t_i - R_i \tilde{t}_{ij}\ _2^2$	$\tau_{ij} \ u_j - u_i - Y_i \tilde{t}_{ij}\ _2^2$
Range	$\sigma_{ij}^{-2} \ t_j - t_i - \tilde{r} b\ _2^2$	$\sigma_{ij}^{-2} \ u_j - u_i - \tilde{r} s\ _2^2$

VIII. EXPERIMENTS

In this section we evaluate the certifiable factor graph optimization framework developed in Section VI on three representative SLAM problem classes (pose graph optimization, landmark SLAM, and range-aided SLAM) using the lifted variable and factor types described in Section VII. For each problem class, we compare our certifiable factor graph-based estimator against the corresponding state-of-the-art hand-crafted certifiable solver to verify that our framework indeed recovers verifiably globally optimal solutions; we also benchmark against standard local factor graph optimization to assess practical efficiency.

A. Common experimental settings

Our certifiable factor graph-based implementation of the Riemannian Staircase (Algorithm 2) is implemented in C++ using GTSAM [37], and employs the Levenberg-Marquardt (LM) algorithm to perform the local factor graph optimization required in line 4 in each iteration. All experiments were conducted on a laptop with an Intel Core i7-11800H CPU and 32 GB RAM, running Ubuntu 22.04.

Certification criterion: Let f^* denote the value of the stationary point recovered from local factor graph optimization in each iteration of Algorithm 2, and S denote the associated certificate matrix. We define an eigenvalue nonnegativity tolerance η according to:

$$\eta := \min\{\eta_{\max}, \max\{10^{-6} f^*, \eta_{\min}\}\}, \quad (58)$$

with $\eta_{\min} = 10^{-3}$ and $\eta_{\max} = 10^{-1}$, and consider the certificate valid if $S + \eta I \succ 0$.

Additional problem-specific settings, including initialization procedures, convergence tolerances, and baseline comparisons, are detailed within each subsection below.

B. Pose graph optimization

In *pose-graph optimization* (PGO), the goal is to jointly estimate a collection of n unknown poses $x_1, \dots, x_n \in \text{SE}(d)$ given a set of noisy pairwise relative measurements $\tilde{x}_{ij} = (\tilde{t}_{ij}, \tilde{R}_{ij}) \in \text{SE}(d)$ between them. This problem can be represented by a directed graph $\mathcal{G} = (\mathcal{V}, \mathcal{E})$, where vertices $\mathcal{V} = [n]$ are in one-to-one correspondence with the unknown poses and edges $\mathcal{E} \subseteq \mathcal{V} \times \mathcal{V}$ are in one-to-one correspondence with the available measurements. Assuming the noise models in (46) and (50), the corresponding maximum likelihood estimation (MLE) problem is:

TABLE II

PGO DATASETS INFORMATION: SUMMARY OF SYNTHETIC AND REAL-WORLD DATASETS, REPORTING THE DIMENSION, NUMBER OF POSES, AND NUMBER OF RELATIVE-POSE MEASUREMENTS.

	Pose Graph Optimization														
	MIT	CSAIL	Intel	Kitti 05	Manhattan	Kitti 00	City	Ais2klinik	Small Grid	Garage	Sphere	Torus	Cubicle	Grid	Rim
Dim	2D	2D	2D	2D	2D	2D	2D	2D	3D	3D	3D	3D	3D	3D	3D
# Poses	808	1045	1728	2761	3500	4251	10000	15115	125	1661	2500	5000	5750	8000	10093
# Measurements	827	1171	2512	2827	5451	4679	20687	16727	297	6275	4949	10000	7696	22236	18637

TABLE III

LANDMARK AND RANGE-AIDED DATASETS INFORMATION: SUMMARY OF REAL-WORLD DATASETS REPORTING THE DIMENSION, NUMBERS OF POSES AND LANDMARKS, AND COUNTS OF RANGE AND RELATIVE-POSE MEASUREMENTS.

	Landmark SLAM		Range-Aided SLAM				
	Victoria [47]	Trees [11]	Goats 16 [48]	Goats 15 [48]	Plaza1 [49]	Plaza2 [49]	Single Drone [31]
Dim	2D	2D	2D	2D	2D	2D	3D
# Poses	6969	10000	201	472	9658	4091	1754
# Landmarks	151	100	4	4	4	4	1
# Measurements	10608	14442	772	1258	12983	5897	3507

Problem 1 (*MLE formulation of PGO*).

$$\min_{t_i \in \mathbb{R}^d, R_i \in \text{SO}(d)} \sum_{(i,j) \in \mathcal{E}} \kappa_{ij} \left\| R_j - R_i \tilde{R}_{ij} \right\|_F^2 + \tau_{ij} \left\| t_j - t_i - R_i \tilde{t}_{ij} \right\|_2^2 \quad (59)$$

Applying the results of Section VI, the lifted version of Problem 1 solved at each instance of the Riemannian Staircase (Algorithm 2) is then:

Problem 2 (*rank- p Burer-Monteiro factorization of PGO*).

$$\min_{t_i \in \mathbb{R}^p, Y_i \in \text{St}(d,p)} \sum_{(i,j) \in \mathcal{E}} \kappa_{ij} \left\| Y_j - Y_i \tilde{R}_{ij} \right\|_F^2 + \tau_{ij} \left\| t_j - t_i - Y_i \tilde{t}_{ij} \right\|_2^2 \quad (60)$$

1) *Experimental setup*: We set `relative_error` to 10^{-5} , `absolute_error` to 10^{-4} , and `max_iteration` to 100. The LM optimizer terminates when either error tolerance is met. We compare against SE-Sync [20], a state-of-the-art, problem-specific certifiable solver for PGO.

2) *Random initialization*: In our first set of experiments, we initialize both our method and SE-Sync by randomly sampling from the appropriate manifolds, with initial rank p_0 equal to the ambient dimension $d \in \{2, 3\}$. For SE-Sync, we employ the translation-explicit formulation in order to enable a fair comparison with our factor graph-based formulation (60). Results from this experiment are shown in Table IV.

Across all datasets, our solver attains the same verifiably globally optimal objective values as SE-Sync. Consistent with [20], the SDP relaxation is tight for the evaluated datasets and noise regimes.

Differences in runtime (see the *Opt. Time* column) primarily stem from algorithmic design: our implementation uses GTSAM’s general-purpose LM with an inexact Hessian and requires relinearization at each iteration, whereas SE-Sync employs a specialized, problem-specific second-order Riemannian trust-region method with analytic derivatives and no relinearization. As a consequence, our approach is generally slower; however, SE-Sync is slower on some real-world datasets (e.g., Garage, Rim, Ais2klinik), while our

method is notably slower on synthetic datasets (e.g., Grid). Note that these randomly-initialized experiments approximate a practical worst-case scenario in terms of both problem difficulty and computation time.

3) *Odometry initialization*: In this set of experiments we initialize all methods using the *odometric* initialization (obtained by concatenating relative pose measurements along the trajectory). For local-search baselines, we run GTSAM’s LM solver with the same hyperparameters as our method to ensure fair comparison.

Table V evaluates efficiency under this informative initialization. Most datasets are solved in comparable total time, and in many cases the algorithm terminates at the initial rank. Nevertheless, even with odometry-based initialization, we observe that local methods may converge to suboptimal solutions. In contrast, our approach recovers certifiably globally optimal solutions in all tested cases.

C. Pose-and-landmark SLAM

Because landmark measurements can be modeled as relative-translation factors (51), we may straightforwardly generalize the PGO formulation (59) to landmark SLAM by applying the same translation factor to pose-landmark measurements.

1) *Experimental setup*: We set `relative_error` to 10^{-5} , `absolute_error` to 10^{-4} , and `max_iteration` to 150. The LM optimizer terminates when either error tolerance is met. We compare against CPL-SLAM [30], specifically using the Landmark-SE-Sync variant provided in their public implementation.

2) *Random initialization*: Both methods are initialized by random sampling from the appropriate manifolds, with initial rank $p_0 = d$. Table IV reports results for Landmark-SE-Sync under random initialization. On both datasets (*Trees*, *Victoria*), our method attains the same verifiably globally optimal objective values as the baseline. Runtime differences are again primarily attributable to differences in solver design as discussed in Section VIII-E.

TABLE IV
RESULTS OF RANDOM INITIALIZATION: OBJECTIVE VALUES AND RUNTIMES ON PGO, LANDMARK SLAM, AND RANGE-AIDED SLAM. WE COMPARE STATE-OF-THE-ART BASELINES (SE-SYNC [20], CPL-SLAM [30], CORA [31]) WITH OUR CERTIFIABLE FACTOR-GRAPH METHODS.

PGO	SE-Sync				Ours			
	Obj. Value	Opt. Time	Tot. Time	Term. Rank	Obj. Value	Opt. Time	Tot. Time	Term. Rank
MIT	6.115×10^1	0.38	0.40	4	6.115×10^1	1.15	1.28	4
CSAIL	3.170×10^1	0.23	0.24	4	3.170×10^1	1.52	1.77	4
Intel	5.235×10^1	3.51	3.57	4	5.235×10^1	5.71	6.13	4
Kitti 05	2.765×10^3	1.31	1.36	5	2.765×10^3	15.58	17.35	4
Manhattan	6.431×10^3	2.38	2.43	3	6.431×10^3	17.12	18.28	4
Kitti 00	1.257×10^2	5.09	5.15	4	1.257×10^2	12.03	15.64	4
City	6.386×10^2	87.16	87.68	4	6.386×10^2	29.85	36.61	4
Ais2klinik	1.886×10^2	900.17	900.40	4	1.886×10^2	106.43	121.59	4
Small Grid	1.025×10^3	0.13	0.13	3	1.025×10^3	0.09	0.09	3
Garage	1.263×10^0	75.58	75.74	5	1.263×10^0	17.06	17.83	5
Sphere	1.687×10^3	14.90	15.03	5	1.687×10^3	8.41	9.67	5
Torus	2.423×10^4	14.53	14.78	5	2.423×10^4	106.71	110.26	5
Cubicle	7.171×10^2	52.09	52.23	4	7.171×10^2	49.61	54.56	5
Grid	8.432×10^4	65.56	68.03	5	8.432×10^4	311.27	318.41	3
Rim	5.461×10^3	357.19	357.67	4	5.461×10^3	130.09	145.62	5

Landmark SLAM	CPL-SLAM				Ours			
	Obj. Value	Opt. Time	Tot. Time	Term. Rank	Obj. Value	Opt. Time	Tot. Time	Term. Rank
Victoria	4.660×10^2	18.68	20.38	4	4.676×10^2	29.21	36.62	4
Trees	6.035×10^2	13.01	14.69	4	6.035×10^2	24.18	28.44	4

Range-Aided SLAM	CORA				Ours					
	SDP Value	Ref. Value	Opt. Time	Tot. Time	Term. Rank	SDP Value	Ref. Value	Opt. Time	Tot. Time	Term. Rank
Goats 16	3.689×10^3	3.894×10^3	0.77	0.80	4	3.709×10^3	3.894×10^3	2.41	2.54	4
Goats 15	1.607×10^4	1.820×10^4	2.37	2.45	5	1.609×10^4	1.820×10^4	3.62	3.71	4
Plaza1	1.291×10^3	1.332×10^3	13.32	14.93	6	1.286×10^3	1.332×10^3	192.18	206.89	5
Plaza2	7.244×10^2	7.343×10^2	4.67	5.06	3	7.259×10^2	7.343×10^2	48.85	51.04	4
Single Drone	7.223×10^0	7.698×10^0	6.63	7.36	4	7.246×10^0	7.698×10^0	21.06	22.30	5

Opt. Time denotes the sum of the optimization times at each level of the Riemannian staircase. **Tot. Time** is the total computation time, including initialization, optimization, verification, saddle-escape, and rounding. **Term. Rank** is the final rank at which the Riemannian staircase terminates. For PGO and landmark-SLAM problems, **Obj. Value** coincides with both the QCQP value (12) and the SDP value (13) due to relaxation tightness under moderate conditions. For range-aided SLAM, since the relaxation is not always tight, we report both the **SDP Value** and the refined solution value **Ref. Value** (see VIII-D).

3) *Odometry initialization*: We initialize robot poses from odometry estimates and landmarks from ground-truth positions (simulating scenarios where landmark positions are approximately known, e.g., from prior mapping or GPS).

Table V summarizes results under strong initialization. On *Trees*, our method achieves runtimes comparable to local-search baselines while additionally providing optimality certificates. On *Victoria*, local methods converge to suboptimal solutions, whereas our approach recovers the globally optimal solution with certification.

D. Range-aided SLAM

Range-aided SLAM extends PGO by incorporating range measurements $\tilde{r}_{ij} \in \mathbb{R}$, modeled by the noise distribution in (54). The objective is to estimate poses $x_1, x_2, \dots, x_n \in \text{SE}(d)$ and landmarks $l_1, l_2, \dots, l_n \in \mathbb{R}^d$ that solve Problem 3.

Problem 3 (*MLE formulation of range-aided SLAM*).

$$\min_{\substack{t_i \in \mathbb{R}^d \\ R_i \in \text{SO}(d)}} \sum_{(i,j) \in \mathcal{E}} \kappa_{ij} \left\| R_j - R_i \tilde{R}_{ij} \right\|_F^2 + \tau_{ij} \|t_j - t_i - R_i \tilde{t}_{ij}\|_2^2 + \frac{1}{\sigma_{ij}^2} (\|t_j - t_i\|_2 - \tilde{r}_{ij})^2 \quad (61)$$

Similarly, the lifted version can be expressed as:

Problem 4 (*rank- p Burer-Monteiro factorization of range-aided SLAM*).

$$\min_{\substack{t_i \in \mathbb{R}^p \\ Y_i \in \text{St}(d,p), (i,j) \in \mathcal{E} \\ b_{ij} \in S^{p-1}}} \sum_{(i,j) \in \mathcal{E}} \kappa_{ij} \left\| Y_j - Y_i \tilde{R}_{ij} \right\|_F^2 + \tau_{ij} \|t_j - t_i - Y_i \tilde{t}_{ij}\|_2^2 + \frac{1}{\sigma_{ij}^2} \|t_j - t_i - \tilde{r}_{ij} b_{ij}\|_2^2 \quad (62)$$

1) *Experimental setup*: Given the poor numerical conditioning of range-aided SLAM, we use stringent stopping cri-

TABLE V

RESULTS OF ODOMETRY INITIALIZATION: OBJECTIVE VALUES AND RUNTIMES ON PGO, LANDMARK SLAM, AND RANGE-AIDED SLAM. WE COMPARE A LOCAL SEARCH-BASED SOLVER (GTSAM [7]) WITH OUR CERTIFIABLE FACTOR-GRAPH METHODS. ALL METHODS ARE INITIALIZED WITH ODOMETRY MEASUREMENTS FOR POSES AND GROUND-TRUTH LANDMARK POSITIONS.

PGO	Ours							GTSAM		
	Obj. Value	Opt. Time	Tot. Time	Init. Rank	Term. Rank	Verif.	Obj. Value	Tot. Time	Verif.	
MIT	6.115×10^1	0.54	0.72	2	4	✓	1.298×10^3	0.17	✗	
CSAIL	3.170×10^1	0.05	0.10	2	2	✓	3.170×10^1	0.06	✓	
Intel	5.235×10^1	0.08	0.21	2	2	✓	5.235×10^1	0.09	✓	
Kitti 05	2.765×10^3	0.33	1.093	2	2	✓	2.765×10^3	0.19	✓	
Manhattan	6.431×10^3	0.46	0.93	2	2	✓	6.431×10^3	0.50	✓	
Kitti 00	1.257×10^2	0.33	1.09	2	2	✓	1.257×10^2	0.37	✓	
City	6.386×10^2	0.60	4.13	2	2	✓	6.386×10^2	0.73	✓	
Ais2klinik	1.886×10^2	114.85	129.37	2	4	✓	1.325×10^3	56.05	✗	
Small Grid	1.025×10^3	0.02	0.02	3	3	✓	1.025×10^3	0.02	✓	
Garage	1.263×10^0	0.17	0.45	3	3	✓	1.263×10^0	0.25	✓	
Sphere	1.687×10^3	0.29	0.86	3	3	✓	1.687×10^3	0.33	✓	
Torus	2.423×10^4	29.40	33.15	3	5	✓	5.276×10^4	5.96	✗	
Cubicle	7.171×10^2	0.89	3.46	3	3	✓	7.171×10^2	1.1	✓	
Grid	8.432×10^4	103.183	110.276	3	3	✓	8.432×10^4	106.85	✓	
Rim	5.461×10^3	2.52	10.86	3	3	✓	5.461×10^3	2.564	✓	

Landmark SLAM	Ours							GTSAM		
	Obj. Value	Opt. Time	Tot. Time	Init. Rank	Term. Rank	Verif.	Obj. Value	Tot. Time	Verif.	
Victoria	4.661×10^2	18.92	25.72	2	4	✓	1.691×10^4	7.34	✗	
Trees	6.036×10^2	0.63	4.52	2	2	✓	6.036×10^2	0.70	✓	

Range-Aided SLAM	Ours							GTSAM		
	SDP Value	Ref. Value	Opt. Time	Tot. Time	Init. Rank	Term. Rank	Verif.	Obj. Value	Tot. Time	Verif.
Goats 16	3.709×10^3	3.894×10^3	2.14	2.26	2	4	✓	4.087×10^5	0.57	✗
Goats 15	1.623×10^4	1.820×10^4	5.56	6.13	2	4	✓	1.665×10^6	0.51	✗
Plaza1	1.289×10^3	1.332×10^3	65.63	73.27	3	4	✓	1.337×10^6	157.99	✗
Plaza2	7.259×10^2	7.343×10^2	50.23	53.37	2	4	✓	3.138×10^5	69.97	✗
Single Drone	7.244×10^0	7.698×10^0	19.07	20.61	3	5	✓	1.867×10^2	2.74	✗

Our method provides certificates of global optimality, whereas the GTSAM local-search solver does not. Accordingly, we apply our certifier to the solutions returned by GTSAM. The verification result column (**Verif.**) reports the certification status for each solution: (✓) indicates a verified globally optimal solution, while (✗) indicates a failure to certify and thus a sub-optimal solution.

teria: `relative_error` and `absolute_error` are both set to 10^{-8} , and `max_iteration` to 300. The LM optimizer terminates when either error tolerance is met. We compare against CORA [31], the state-of-the-art certifiable solver for range-aided SLAM.

Remark 2 (Range-aided SLAM tolerances): Range measurements are scalar and typically constrain the state only weakly, contributing limited information to the system. Consequently, the information matrix is often ill-conditioned and the objective may exhibit broad flat regions. In such regimes, Gauss-Newton or LM may produce only marginal decreases in the cost even far from optimality, so loose tolerances can trigger premature termination. To mitigate this, we adopt *tight* tolerances (relative and absolute errors on the order of 10^{-8}) and a higher iteration cap (300), permitting more stringent local optimizations that can help to escape flat regions in the

loss landscape.

2) *Random initialization:* Both methods are initialized by random sampling from the appropriate manifolds, with initial rank $p_0 = d$. Table IV reports results under random initialization. Because the relaxation is not always exact for range-aided problems (as observed in [31]), an optimality gap can arise between the Shor relaxation and the optimal value of the original MLE. Consequently, both CORA [31] and our certifiable factor graph-based RA-SLAM estimator perform a final *solution refinement* step that projects the SDP solution onto the feasible set of the original problem and then performs a final *local* optimization: we report the refined objective values as *Refined Obj. Val.*, and the pre-refinement SDP values as *SDP Obj. Val.*

We observe that the final SDP objective values obtained by our approach are slightly higher than CORA’s [although

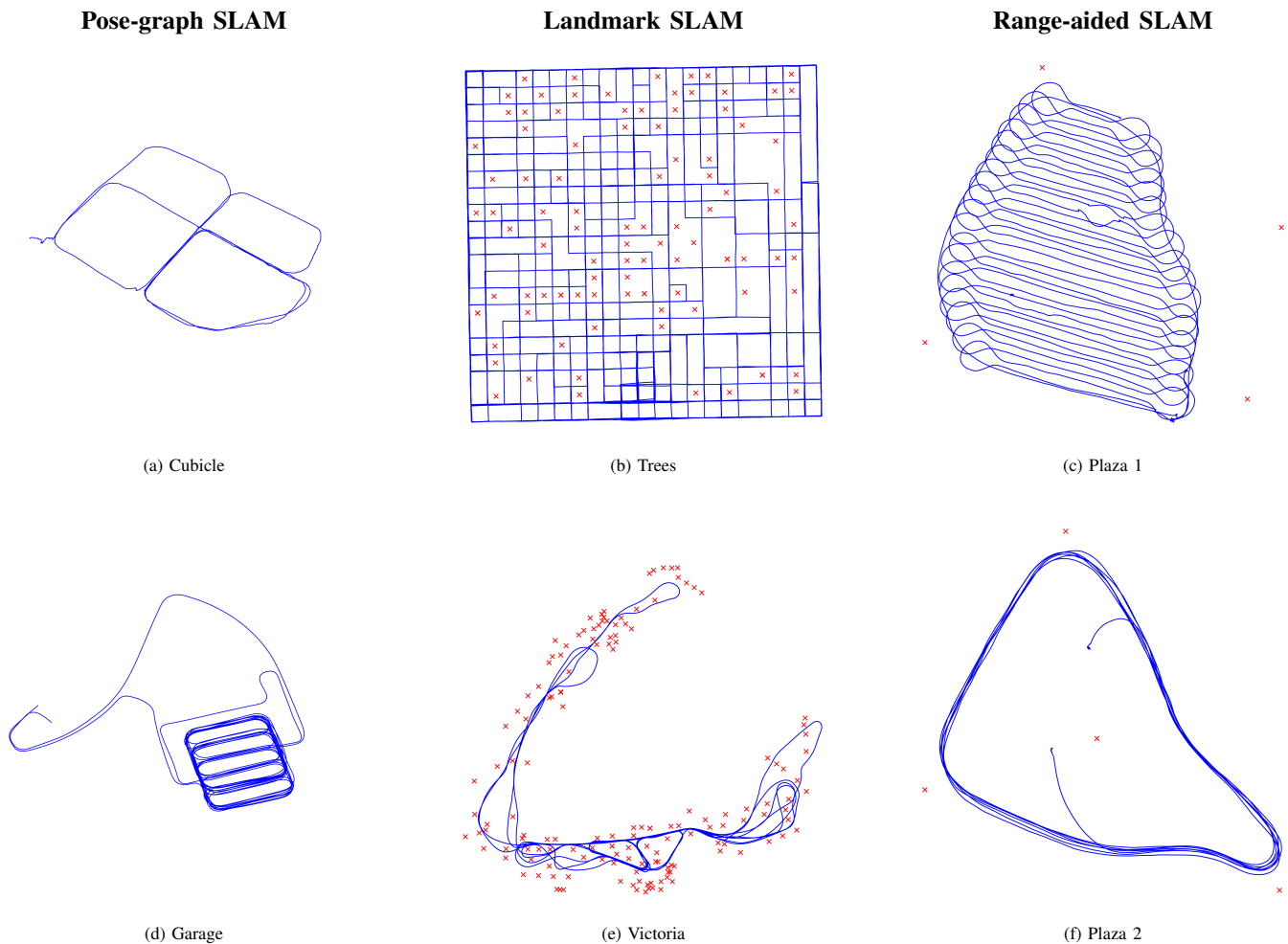


Fig. 3: Globally optimal results on select SLAM benchmark datasets encompassing pose-graph optimization, landmark, and range-aided problems. The blue denotes the trajectory that the robot traversed, while the red denotes the landmarks utilized in the case of landmark and range-aided SLAM.

they are still certified as (numerically) globally optimal using the numerical eigenvalue nonnegativity test described in [58]. This discrepancy in the final objective values stems from the slower convergence of a general-purpose LM algorithm compared to CORA’s truncated-Newton Riemannian trust-region (RTR) method, especially in the presence of ill-conditioned lifted range factors. As a consequence, our solver often climbs to higher BM ranks before certification is achieved. Since both approaches share the same SDP-based initialization, the refined objective values coincide. In runtime, our method is significantly slower on certain datasets, primarily due to the LM solver’s inefficiency on ill-conditioned problem instances.

3) *Odometry initialization*: We initialize robot poses from odometry estimates and, where applicable, landmarks from ground-truth positions.

Table V summarizes results under strong initialization. Notably, no local method produced a certifiably globally optimal solution on the range-aided SLAM tasks, indicating that local optimization can stall at suboptimal minima even with good initial guesses. By contrast, our approach returns certified globally optimal solutions.

E. Discussion

1) *Numerical performance*: Across all benchmarks, our certifiable factor-graph approach recovers solutions that are indistinguishable (up to numerical tolerances) from those produced by state-of-the-art hand-crafted certifiable solvers. This is expected, since all of these approaches are ultimately solving the same underlying SDP relaxations.

Our method is often, although not always, slower to converge than these custom-built solvers. This is also unsurprising: the comparison baselines are all based upon hand-crafted, highly optimized, *problem-specific* optimization algorithms, whereas our pipeline deliberately uses a general-purpose backend. In particular, the baselines all employ *exact* Riemannian Hessians, whereas we rely upon GTSAM’s Levenberg-Marquardt method, which is based upon a regularized Gauss-Newton Hessian approximation whose quality is known to degrade in the presence of either large measurement residuals or strong objective curvature, both of which are common features of practical SLAM problems [12].⁹

⁹Indeed, we observe that the performance gap is most pronounced in range-aided SLAM, where poor numerical conditioning amplifies the difference between the exact Riemannian Hessian and its LM approximation.

We emphasize that this runtime gap is not a fundamental limitation of our certifiable factor graph framework, but rather a consequence of deliberately prioritizing generality and ease of use over highly-optimized, problem-specific implementations. This gap could be further narrowed by developing dedicated solvers tailored to certifiable estimation within the general-purpose factor graph paradigm, a direction that we leave for future work.

2) *Implementation effort and practicality*: The computational issues discussed above must be weighed against the dramatic reduction in implementation effort enabled by our certifiable factor graph framework, a comparison that overwhelmingly favors our approach. At present, designing and deploying a new certifiable estimator is a laborious and highly specialized undertaking: practitioners must manually analyze the estimation problem, derive an associated effective SDP relaxation, construct the corresponding Burer-Monteiro factorization, design a custom Riemannian optimization algorithm for the BM-factored SDP relaxation that is tailored to the specific geometry of the problem’s feasible set, and then wrap the entire pipeline in a Riemannian Staircase meta-algorithm. Each of these steps requires substantial expertise in convex analysis, differential geometry, and numerical optimization, and must be repeated *ab initio* for every individual problem class one wants to address. According to reports from the authors of the state-of-the-art certifiable estimators used as the baselines in our experiments (personal communication), the initial development of each of these custom certifiable solvers required *several weeks to months* of dedicated engineering effort, even for practitioners with substantial prior expertise and experience in convex optimization, differential geometry, and numerical methods.

In contrast, assembling a certifiable estimator using our certifiable factor graph framework can typically be completed in a *day or less*. A practitioner already familiar with standard factor graph optimization need only replace the original variable and factor types appearing in their existing factor graph model with their lifted certifiable counterparts; the rest follows automatically from the framework developed in this paper. In particular, no specialized expertise in convex optimization, semidefinite programming, or differential geometry is required, and no custom solver development is needed. This reduction in implementation effort, from weeks or months to hours, is the central practical contribution of this work, and paves the way for certifiable estimation to become as ubiquitous in robotic perception as conventional factor graph optimization is today.

IX. CONCLUSIONS

In this work, we have demonstrated that certifiable estimators can be implemented and deployed within existing factor-graph modeling and optimization libraries (e.g., GTSAM) by leveraging a key theoretical insight: the correspondence between quadratically constrained quadratic programs (QCQPs) and factor-graph representations. This connection is instantiated through rank- p BM factorization, enabling seamless integration of the Riemannian staircase and certification mechanisms within standard factor-graph optimization back-ends.

The resulting framework is simplified, modular, and practical: certifiable algorithms become as easy to run as standard local-search methods over factor graphs, making them suitable as plug-and-play state-estimation modules in real-world robotic systems.

Concretely, we introduce *lifted variables* and propose *lifted factors* for commonly used measurement types. These components can be assembled with minimal effort into three representative SLAM examples—pose-graph optimization, landmark-based SLAM, and range-aided SLAM—and benchmarked against state-of-the-art hand-crafted certifiable solvers, all within a practical, plug-and-play system compatible with off-the-shelf libraries (e.g., GTSAM). We validate the framework through extensive experiments on both synthetic and real-world SLAM datasets. Moreover, the proposed approach facilitates rapid prototyping of new certifiable estimation problems by allowing users to introduce new lifted factors for a wide variety of sensor measurements.

A key contribution of this work is the substantial reduction in implementation effort and the corresponding lowering of the barrier to entry: certifiable estimation becomes as accessible as standard factor-graph optimization. Whereas prior custom pipelines often require weeks to months of engineering per problem class, our plug-and-play factors enable users to assemble a certifiable estimation pipeline in less than a day. This reduction *democratizes access* to certifiably correct estimation for non-experts, simplifies deployment in robotic systems already using factor graphs, and provides researchers with a lightweight on-ramp for rapid experimentation. By enabling practitioners familiar with traditional SLAM back-ends to incorporate global optimality guarantees with minimal effort, our framework aims to stimulate further advances in certifiable state estimation. Future work will explore extending the proposed certifiable factors to a broader class of robotic estimation problems, including real-robot deployment and field robotics experiments.

REFERENCES

- [1] S. Thrun, “Probabilistic robotics,” *Communications of the ACM*, vol. 45, no. 3, pp. 52–57, 2002.
- [2] T. D. Barfoot, *State Estimation for Robotics*. Cambridge University Press, 2017.
- [3] C. Cadena, L. Carlone, H. Carrillo, Y. Latif, D. Scaramuzza, J. Neira, I. Reid, and J. J. Leonard, “Past, present, and future of simultaneous localization and mapping: Toward the robust-perception age,” *IEEE Transactions on Robotics*, vol. 32, no. 6, pp. 1309–1332, 2016.
- [4] D. M. Rosen, K. J. Doherty, A. Terán Espinoza, and J. J. Leonard, “Advances in inference and representation for simultaneous localization and mapping,” *Annual Review of Control, Robotics, and Autonomous Systems*, vol. 4, no. 1, pp. 215–242, 2021.
- [5] J. L. Schonberger and J.-M. Frahm, “Structure-from-motion revisited,” in *IEEE Conference on Computer Vision and Pattern Recognition (CVPR)*, 2016, pp. 4104–4113.
- [6] F. Dellaert, M. Kaess *et al.*, “Factor graphs for robot perception,” *Foundations and Trends® in Robotics*, vol. 6, no. 1-2, pp. 1–139, 2017.
- [7] F. Dellaert and G. Contributors, “borglab/gtsam,” May 2022. [Online]. Available: <https://github.com/borglab/gtsam>
- [8] R. Kümmerle, G. Grisetti, H. Strasdat, K. Konolige, and W. Burgard, “g2o: A general framework for graph optimization,” in *IEEE International Conference on Robotics and Automation (ICRA)*. IEEE, 2011, pp. 3607–3613.
- [9] S. Agarwal, K. Mierle *et al.*, “Ceres solver: Tutorial & reference,” *Google Inc*, vol. 2, no. 72, p. 8, 2012.
- [10] J. Nocedal and S. J. Wright, *Numerical Optimization*. Springer, 1999.

- [11] M. Kaess, H. Johannsson, R. Roberts, V. Ila, J. J. Leonard, and F. Dellaert, "iSAM2: Incremental smoothing and mapping using the bayes tree," *The International Journal of Robotics Research*, vol. 31, no. 2, pp. 216–235, 2012.
- [12] D. M. Rosen, M. Kaess, and J. J. Leonard, "Rise: An incremental trust-region method for robust online sparse least-squares estimation," *IEEE Transactions on Robotics*, vol. 30, no. 5, pp. 1091–1108, 2014.
- [13] L. Carlone, R. Tron, K. Daniilidis, and F. Dellaert, "Initialization techniques for 3D SLAM: A survey on rotation estimation and its use in pose graph optimization," in *IEEE International Conference on Robotics and Automation (ICRA)*. IEEE, 2015, pp. 4597–4604.
- [14] M. Todd, "Semidefinite optimization," *Acta Numerica*, vol. 10, pp. 515–560, 2001.
- [15] S. Burer and R. D. Monteiro, "A nonlinear programming algorithm for solving semidefinite programs via low-rank factorization," *Mathematical Programming*, vol. 95, no. 2, pp. 329–357, 2003.
- [16] N. Boumal, V. Voroninski, and A. Bandeira, "The non-convex Burer-Monteiro approach works on smooth semidefinite programs," *Advances in Neural Information Processing Systems*, vol. 29, 2016.
- [17] N. Boumal, *An introduction to optimization on smooth manifolds*. Cambridge University Press, 2023.
- [18] J. Nocedal and S. J. Wright, *Numerical Optimization*, 2nd ed., ser. Springer Series in Operations Research and Financial Engineering. New York: Springer, 2006.
- [19] M. Kaess, A. Ranganathan, and F. Dellaert, "iSAM: Incremental smoothing and mapping," *IEEE Transactions on Robotics*, vol. 24, no. 6, pp. 1365–1378, 2008.
- [20] D. M. Rosen, L. Carlone, A. S. Bandeira, and J. J. Leonard, "SE-Sync: A certifiably correct algorithm for synchronization over the special Euclidean group," *The International Journal of Robotics Research*, vol. 38, no. 2-3, pp. 95–125, 2019.
- [21] J. Briaies and J. Gonzalez-Jimenez, "Cartan-sync: Fast and global se (d)-synchronization," *IEEE Robotics and Automation Letters*, vol. 2, no. 4, pp. 2127–2134, 2017.
- [22] A. Eriksson, C. Olsson, F. Kahl, and T.-J. Chin, "Rotation averaging and strong duality," in *IEEE Conference on Computer Vision and Pattern Recognition (CVPR)*, 2018, pp. 127–135.
- [23] M. ApS, *The MOSEK optimization toolbox for MATLAB manual. Version 9.0.*, 2019. [Online]. Available: <http://docs.mosek.com/9.0/toolbox/index.html>
- [24] S. J. Wright, *Primal-dual interior-point methods*. SIAM, 1997.
- [25] G. Grisetti, R. Kümmerle, C. Stachniss, and W. Burgard, "A tutorial on graph-based slam," *IEEE Intelligent Transportation Systems Magazine*, vol. 2, no. 4, pp. 31–43, 2011.
- [26] S. Agarwal, N. Snavely, S. M. Seitz, and R. Szeliski, "Bundle adjustment in the large," in *European Conference on Computer Vision ECCV*. Springer, 2010, pp. 29–42.
- [27] A. A. Ahmadi and A. Majumdar, "DSOS and SDSOS optimization: More tractable alternatives to sum of squares and semidefinite optimization," *SIAM Journal on Applied Algebra and Geometry*, vol. 3, no. 2, pp. 193–230, 2019.
- [28] S. Boyd, N. Parikh, E. Chu, B. Peleato, and J. Eckstein, "Distributed optimization and statistical learning via the alternating direction method of multipliers," *Foundations and Trends in Machine Learning*, vol. 3, no. 1, pp. 1–122, 2011.
- [29] C. Holmes and T. D. Barfoot, "An efficient global optimality certificate for landmark-based SLAM," *IEEE Robotics and Automation Letters*, vol. 8, no. 3, pp. 1539–1546, 2023.
- [30] T. Fan, H. Wang, M. Rubenstein, and T. Murphey, "CPL-SLAM: Efficient and certifiably correct planar graph-based SLAM using the complex number representation," *IEEE Transactions on Robotics*, vol. 36, no. 6, pp. 1719–1737, 2020.
- [31] A. Papalía, A. Fishberg, B. W. O'Neill, J. P. How, D. M. Rosen, and J. J. Leonard, "Certifiably correct range-aided slam," *IEEE Transactions on Robotics*, vol. 40, pp. 4265–4283, 2024.
- [32] Y. Tian, K. Khosoussi, D. M. Rosen, and J. P. How, "Distributed certifiably correct pose-graph optimization," *IEEE Transactions on Robotics*, vol. 37, no. 6, pp. 2137–2156, 2021.
- [33] Y. Tian, Y. Chang, F. H. Arias, C. Nieto-Granda, J. P. How, and L. Carlone, "Kimera-multi: Robust, distributed, dense metric-semantic SLAM for multi-robot systems," *IEEE Transactions on Robotics*, vol. 38, no. 4, 2022.
- [34] P.-A. Absil, R. Mahony, and R. Sepulchre, *Optimization algorithms on matrix manifolds*. Princeton University Press, 2008.
- [35] F. Dellaert, D. M. Rosen, J. Wu, R. Mahony, and L. Carlone, "Shonan rotation averaging: Global optimality by surfing $SO(p)^n$," in *European Conference on Computer Vision (ECCV)*, Aug. 2020.
- [36] P. Huber, *Robust Statistics*. Hoboken, N.J.: John Wiley & Sons, 2004.
- [37] F. Dellaert, "Factor graphs and GTSAM: A hands-on introduction," Institute for Robotics & Intelligent Machines, Georgia Institute of Technology, Tech. Rep. GT-RIM-CP&R-2012-002, Sep. 2012.
- [38] T. Ferguson, *A Course in Large Sample Theory*. Boca Raton, FL: Chapman & Hall/CRC, 1996.
- [39] N. Z. Shor, "Quadratic optimization problems," *Soviet Journal of Computer and Systems Sciences*, vol. 25, pp. 1–11, 1987.
- [40] F. A. Potra and S. J. Wright, "Interior-point methods," *Journal of computational and applied mathematics*, vol. 124, no. 1-2, pp. 281–302, 2000.
- [41] D. M. Rosen, "Scalable low-rank semidefinite programming for certifiably correct machine perception," in *International Workshop on the Algorithmic Foundations of Robotics*. Springer, 2020, pp. 551–566.
- [42] D. Cifuentes, S. Agarwal, P. A. Parrilo, and R. R. Thomas, "On the local stability of semidefinite relaxations," *Mathematical Programming*, vol. 193, no. 2, pp. 629–663, 2022.
- [43] S. P. Boyd and L. Vandenberghe, *Convex optimization*. Cambridge university press, 2004.
- [44] N. Boumal, "A riemannian low-rank method for optimization over semidefinite matrices with block-diagonal constraints," *arXiv preprint arXiv:1506.00575*, 2015.
- [45] N. Boumal, B. Mishra, P.-A. Absil, and R. Sepulchre, "Manopt, a MATLAB toolbox for optimization on manifolds," *Journal of Machine Learning Research*, vol. 15, no. 1, pp. 1455–1459, 2014.
- [46] T. Halsted and M. Schwager, "The riemannian elevator for certifiable distance-based localization," *Preprint*, 2022.
- [47] J. E. Guivant and E. M. Nebot, "Optimization of the simultaneous localization and map-building algorithm for real-time implementation," *IEEE transactions on robotics and automation*, vol. 17, no. 3, pp. 242–257, 2002.
- [48] E. Olson, J. J. Leonard, and S. Teller, "Robust range-only beacon localization," *IEEE Journal of Oceanic Engineering*, vol. 31, no. 4, pp. 949–958, 2007.
- [49] J. Djugash, B. Hamner, and S. Roth, "Navigating with ranging radios: Five data sets with ground truth," *Journal of Field Robotics*, vol. 26, no. 9, pp. 689–695, 2009.